ASTRONOMY & ASTROPHYSICS
SUPPLEMENT SERIES

Astron. Astrophys. Suppl. Ser. **117**, 417-444 (1996)

Near-infrared surface photometry of spiral galaxies.⋆,⋆⋆ I. The data

Ph. Héraudeau[1], F. Simien[1] and G.A. Mamon[2,3]

[1] Observatoire de Lyon, F-69561 Saint-Genis-Laval Cedex, France
[2] Institut d'Astrophysique (CNRS), 98 bis boulevard Arago, F-75014 Paris, France
[3] DAEC, Observatoire de Paris, F-92195 Meudon, France

Received May 17; accepted November 22, 1995

Abstract. — We present K'-band surface photometry of a sample of 31 inclined Sa-Scd galaxies, together with additional J- and H-band data for four of them. In this first paper of a series, profiles are presented, together with global and isophotal parameters. Our profiles are compared to similar B, R and I data collected from other sources. Three galaxies exhibit previously unknown small bars in their center, while in five others, such bars may also be present. Four objects present a narrow elongated feature in their center aligned with their major axis, which could be an inward extension of the disk. A few galaxies display very thin spiral arms. Color-color diagrams indicate that the extinction inside the four galaxies for which we have JHK' images is limited to $A_V < 2$.

Key words: galaxies: spiral — galaxies: photometry — infrared: galaxies

1. Introduction

The recent availability of near-infrared (NIR) arrays and their continuous improvement have resulted in a fast growing amount of published surface-photometry data on spiral galaxies (de Jong & van der Kruit 1994; Peletier et al. 1994; Terndrup et al. 1994; McLeod & Rieke 1995; Rauscher 1995, to cite only a few recent works dealing with sizable samples). This paper is the first in a series dedicated to the study of several structural and kinematical aspects of spirals in a wide range of Hubble types; it is mainly limited to the reduction of the surface photometry and to the discussion of morphological aspects. It is organized as follows: sample selection, observational procedures and preliminary reductions are presented in Sect. 2, with complementary data in other bandpasses (collected from the literature) described in Sect. 3. Section 4 compares our photometry with that of other sources, sums up the main morphological properties, and discusses briefly color-color diagrams for the four objects observed in three passbands; the last subsection is a discussion which presents the planned applications, mainly the decomposition into the main stellar components and the derivation of mass models.

2. Observations and data reductions

2.1. *Sample*

As part of a wider program of surface photometry observations on nearby galaxies, we have selected an initial sample of southern, unbarred galaxies from the following criteria: i) a morphological type from Sa to Scd, ii) an absolute magnitude $M_B < -19$ and a distance $\Delta < 53.3$ Mpc (with $H_0 = 75\,\mathrm{km\,s^{-1}\,Mpc^{-1}}$, this corresponds to a radial velocity $cz < 4000\,\mathrm{km\,s^{-1}}$, after a correction of 220 km s^{-1} for the Virgocentric infall, from Tammann & Sandage 1985), iii) an inclination angle $45° < i < 78°$ (based on an outer axial ratio $0.21 < R_{25} < 0.71$), iv) an apparent diameter $D_{25} < 5.5'$, and v) coordinates restricted to $-72° < \delta < 0°$, with a zone of avoidance at $|b_{\rm II}| < 20°$.

This first selection brought out 168 galaxies. Telescope availability for a single run cut down to 93 the number of observable objects, still representing a volume-limited sample; 31 objects were actually observed, among which 22 strictly meet the criteria above, while nine other galaxies were added for their specific interest, although they were up to 17% fainter than the limit $M_B = -19$ and/or at moderate northern declination. Histograms of the main characteristic parameters showed that the distribution

Send offprint requests to: F. Simien (simien@obs.univ-lyon1.fr)
⋆Based in part on observations collected at the European Southern Observatory, La Silla, Chile
⋆⋆Tables 2a and 2b are presented in electronic form only; Tables 1 through 3 are available from the CDS, Strasbourg (anonymous ftp to 130.79.128.5)

within the observed set does not differ fundamentally from that in the selected sample, except for a deficiency of far-away objects; in contrast, our set includes more small-D_{25} objects than the sample limited by $cz < 3200\,\mathrm{km\,s^{-1}}$. To sum up, our observed set of 31 galaxies constitutes only marginally a statistically homogeneous sample.

2.2. *Observations*

We used the IRAC2-A camera equipped with a NICMOS3 256×256 detector, attached to the ESO/MPI 2.2-m telescope at La Silla, Chile, between July 5 and 9, 1993. This instrument has been extensively tested and described (for details, see, e.g., Moorwood et al. 1992). All 31 galaxies were observed in the K' filter (2.1 μm), located slightly shortward of the standard K passband in order to reduce the thermal background (Wainscoat & Cowie 1992); four of these objects, selected for their appropriate dimensions and orientation, were, in addition, observed in the J (1.25 μm) and H (1.65 μm) bands, with the aim of getting some insight in dust obscuration, through two-color indices.

For the camera magnification, we selected objective C, which appeared to be the best suited to our program, in terms of compromise between resolution, field, and flatness of response: with this setting, the field was $125 \times 125''$, and the pixel size $0.49''$.

For good sky subtraction, several galaxy (G) and sky (S) exposures were made for each object, in S-G-S sequences. The different galaxy frames were shifted in position by a few arcsec for a better correction of bad pixels on the resulting, average frame; a few large objects are actually a mosaic of frames separated by a fraction of an arcmin. Typical individual exposure times on a galaxy ranged from 5 to 12 seconds, for a total of $\approx 10-20$ minutes: the cumulated on-object exposure times in K' are listed in Table 1. For the four galaxies also observed in J and H, they were 30–40% shorter than the K' time (this difference was motivated by the high luminosity of these objects); these shorter integrations do not reflect into statistically larger error bars in the profiles of Fig. 4: these errors are even often smaller (especially in J), due to the fainter sky brightness with respect to K', but we note a lesser typical quality for the H-band data. The successive sky frames were separated by less than five minutes in time, and several locations were selected around the galaxy, at a few arcmin from its center. The integration time on sky was either the same as on the object, or half that amount.

During our four-night run, about one night was lost due to poor weather. On another night, some thin cirrus was present close to a few objects, making flatfielding difficult and calibration uncertain (details are given in Appendix A: comments on individual objects). The observations of standard stars were also used to monitor the atmospheric transparency (see Sect. 2.3). On the whole, the seeing conditions, as measured by a two-gaussian fit to star images, ranged from $1.0''$ to $2.0''$ (FWHM).

2.3. *Preliminary reductions*

1. Flatfielding: we adopted as the standard flatfield the difference between frames on the dome obtained, successively, with and without illumination by a tungsten source; this procedure allowed to remove the large dark ring present on every single frame of IRAC2-A, and, more generally, all "dark current" manifestations. Several such exposures were made at the beginning and at the end of each night. A couple of bands with a slightly different mean brightness were also present on the raw frames, and their contrast turned out to be sometimes variable; so, when processing images for which this was noticed, the dome flatfield was replaced by a neighboring sky frame, close to the galaxy frame in both time and position. At this stage, we noticed $\approx 0.5\%$ of bad pixels on the detector.
2. Sky brightness determination: in the standard procedure, i.e., when using the dome flatfields, and after dividing all frames by these, we subtracted from the galaxy a mean of neighboring sky frames. On the resulting, average galaxy frame, we measured the background in several outer areas, and from its dispersion we estimated the degree of flatness: it was, typically, better than 0.07% of the sky level. Figure 1 presents the variations of the mean sky level in the K' band, from the beginning to the end of our run; this monitoring was made by collecting all the average sky brightnesses for the observed galaxies, corrected to the same airmass ($= 1.0$). For each night, it is worth noting that the trend toward a darker level at the middle of the night is $\simeq 0.5$ mag arcsec^{-2}; the sky color indices are $J - H \simeq 2.0$ and $H - K' \simeq 0.4$.
3. Photometric calibration: we used faint stars from the list of Carter (1993), and our magnitudes are thus consistent with the SAAO system; during the three clear nights, at airmasses between 1.0 and 2.0, we observed either four or five stars, each one with its image successively in five different locations on the detector. The calculated extinction coefficients have mean values of 0.14 in J, 0.10 in H, and 0.11 in K', not inconsistent with other observations at La Silla (Engels et al. 1981; Bersanelli et al. 1991). With these data, we estimate the uncertainty of our calibrations to be $\simeq 0.05$ mag. For the calibration stars, photometric corrections from K to K' were made according to Wainscoat & Cowie (1992).

2.4. *Isophote analysis*

On the calibrated images, stars were removed, if any, and the ellipse-fitting program of the ESO-Midas reduction software was run, resulting in values of the following

parameters: brightness level μ, ellipticity ϵ ($\equiv 1-$ axial ra tio), and position angle PA at a range of semi-major ax r. The values of PA and ϵ listed in Table 3 correspond t $\mu_{K'} = 19.5$. At faint levels, μ was determined by integra ing within elliptical annuli of increasing "thickness"; fc the outermost isophotes, fixed ellipticity and orientatic were assumed, so as to lower the uncertainty on μ.

In addition, we analyzed the departure of isophot shapes from perfect ellipses, in the inner region where th is relevant to the detection of bars, and disky, boxy, or tr axial structures. We adopted the technique of Michard Simien (1988), and we parameterized an isophote shaj (assumed to be symmetric) by the Fourier coefficients e_4, e_6, and e_8. Although not strictly identical to the well-known coefficient a_4, our e_4 describes the isophotes in the same way, with positive and negative values referring, respectively, to "disky" and "boxy" shapes. Needless to say, this analysis requires much better data than the simple ellipse fitting, and we limited ourselves to: a) galaxies for which this was possible well outside the central region dominated by resolution effects, and b) regions where the isophotes appeared reasonably symmetric, free from chaotic distortions. The analysis has been possible on 12 of our sample galaxies. Figure 4 presents the e_4 profiles, together with the e_6 for the four large galaxies observed in the three passbands; Table 2b lists e_4 through e_8 (e_4 alone is sometimes insufficient for the reconstruction of the isophote, higher-order terms are then used, usually up to e_6 or e_8).

2.5. *Determination of integrated luminosities*

The total luminosity of each galaxy is computed by extrapolating exponential models, adapted to the measured outer profiles, beyond the range of reliable isophote analyses, using fixed isophote ellipticities and orientations. Tests show that the uncertainties on the integrated luminosities are $\simeq 0.1$ mag.

2.6. *Comments on individual galaxies*

Miscellaneous remarks on either the morphology, the photometric characteristics, or peculiarities appeared during the reduction procedure are presented in Appendix A.

3. Additional surface-photometry data

With the aim of making relevant comparisons, we also collected available surface-photometry data in other passbands for our sample galaxies. The sources are the following:

1. B- and R-band images were requested from the ESO-LV database (Lauberts & Valentijn 1989); for these, the pixel size is $1.35''$ and the seeing conditions were from $2''$ to $3''$ (FWHM). The images were available for 20 of our galaxies; they come from scans on Schmidt plates and, expectedly, many of them lack the high S/N ratio of recent CCD data, especially the B frames, but they are still valuable for bringing out extinction effects. Since offsets have been reported in the photometric calibration of some of these images (Huizinga 1994; Peletier et al. 1994), we made careful checks; indeed, for 14 out of 20, we noticed a discrepancy between the sky brightnesses indicated in the headers of the images, and the values that we actually measured within selected areas. We found a mean magnitude difference of 0.23 ± 0.01 in B and 0.13 ± 0.02 in R (the sky measured on the images being fainter), thus confirming values given by the above-cited authors. For nine galaxies, aperture-photometry from the catalogs of Longo & de Vaucouleurs (1983) and de Vaucouleurs & Longo (1988) allowed a direct re-calibration; for the others, we have assumed that the sky brightness of the header was correct (we note that Peletier et al. assumed instead that the value given in the ESO-LV catalog was correct), and we have re-calibrated accordingly. After these corrections, the ellipse-fitting program was run, resulting in the adopted B and R profiles.
2. For 10 galaxies, I-band data were obtained from Mathewson et al. (1992). These authors indicate that most of their galaxies with $D_{25} \lesssim 5'$ were observed with a pixel size of $0.56''$, and they do not specify their typical seeing dimension. They determined the photometric profiles from ellipse fitting to the isophotes; their magnitudes, in the Kron-Cousins system, are estimated accurate to within 0.05 mag.
3. Data from the Haute-Provence Observatory: in their visible- and I-band surface photometry, Héraudeau & Simien (1996: hereafter HS96) have four objects in common with the present sample; their data are in the Kron-Cousins system and have been obtained with a pixel size of $0.78''$. For NGC 7541 their B image, and V and I profiles (seeing conditions of $2.5''$) are

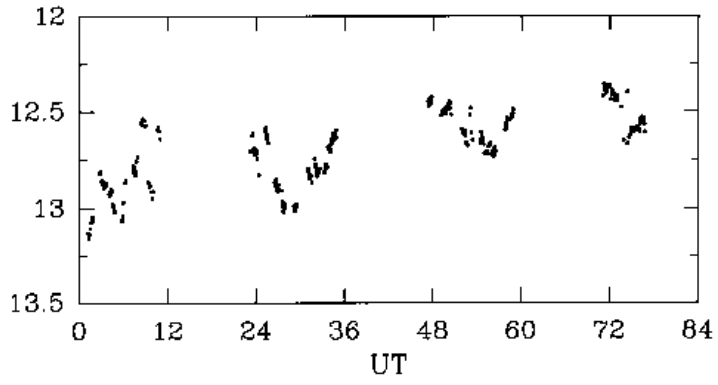

Fig. 1. Variation of the K'-band brightness of the night sky during the four-night run. Abscissae give UT starting on July 5, 1993

Table 1. Catalog elements and exposure times for observed galaxies

#	object		T	α_{1950}	δ_{1950}	B_T	D_{25}	cz	Δ	exp
(1)	(2)	(3)	(4)	(5)	(6)	(7)	(8)	(9)	(10)	(11)
1	E 320-26		3	11 47 19.0	−38 30 24	12.84	2.4	2835	35.7	768
2	E 380-06		3	12 12 57.0	−35 21 06	12.66	3.7	2943	37.4	720
3	E 267-37	N 4219	4	12 13 50.0	−43 02 48	12.71	4.2	1986	24.2	800
4	E 322-28		2	12 32 04.0	−42 15 24	14.41	1.4	3715	47.4	1200
5	E 323-38		6	12 51 30.4	−41 33 04	14.31	1.3	3339	42.5	1200
6		N 5119	5	13 21 21.5	−12 00 58	13.07	1.3	2857	38.1	1200
7		N 5604	1	14 22 06.9	−02 59 12	13.54	1.8	2747	37.4	900
8		M -2-38-22	3	14 49 28.1	−10 32 11	14.01	1.6	2587	34.8	1200
9		M -1-39-05	2	15 20 42.8	−03 58 30	13.65	1.6	1999	27.5	1200
10		N 5937	3	15 28 09.9	−02 39 35	12.71	1.8	2805	38.4	1200
11		N 6063	6	16 04 48.1	+08 06 40	13.67	1.7	2847	39.7	1200
12	E 139-11		2	17 31 52.0	−58 13 24	14.22	1.5	2736	33.9	600
13	E 140-24	I 4717	3	18 28 58.0	−58 00 42	14.16	1.5	3168	39.6	960
14	E 184-17	I 4821	5	19 05 27.0	−55 05 48	13.65	1.8	2698	33.4	1200
15	E 184-27	I 4826	2	19 08 08.0	−57 17 06	14.47	1.4	3459	43.5	1200
16	E 184-67	N 6788	2	19 22 47.0	−55 03 06	12.87	2.9	3168	39.7	800
17	E 142-35	N 6810	2	19 39 21.0	−58 46 30	12.35	3.0	1941	23.1	800
18	E 073-22	I 4929	3	20 01 14.0	−71 49 30	14.33	1.4	4194	52.6	1200
19	E 233-41	N 6870	2	20 06 33.0	−48 26 06	13.18	2.6	2620	32.6	750
20	E 399-25		1	20 10 11.0	−37 20 24	13.78	2.2	2540	32.2	1200
21	E 287-13		4	21 19 56.0	−45 59 12	13.01	2.9	2695	33.5	960
22	E 107-36	N 7083	5	21 31 50.0	−64 07 42	11.90	3.6	3111	38.2	840
23	E 466-38	N 7172	1	21 59 07.0	−32 06 36	12.80	2.4	2566	32.4	900
24		N 7328	2	22 34 59.8	+10 16 23	13.96	2.1	2824	38.4	1200
25	E 290-29	I 5267	1	22 54 22.0	−43 39 48	11.31	5.4	1714	20.2	600
26	E 406-34	I 5271	3	22 55 16.0	−34 00 36	12.47	2.6	1720	20.8	1200
27		N 7537	4	23 12 01.9	+04 13 33	13.86	2.1	2675	35.8	900
28		N 7541	4	23 12 10.3	+04 15 43	12.42	3.3	2682	35.9	600
29		N 7606	3	23 16 29.2	−08 45 33	11.51	4.8	2232	29.0	1200
30	E 605-07	I 5321	1	23 23 43.0	−18 13 48	13.96	1.2	2867	36.8	720
31		N 7721	5	23 36 14.1	−06 47 43	12.22	3.0	2013	26.1	600

Columns:
(1)-(3) galaxy identification
(4) T: morphological type
(5), (6) coordinates
(7) B_T: integrated blue magnitude
(8) D_{25}: apparent diameter at brightness level $\mu_B = 25$, in arcmin
(9) cz: heliocentric radial velocity in $\mathrm{km\,s^{-1}}$
(10) Δ: distance in Mpc (with $H_0 = 75\,\mathrm{km\,s^{-1}\,Mpc^{-1}}$), from cz corrected for Virgocentric infall
(11) exp: total K' exposure time, in seconds
Note: Cols. (4) to (9) are from the *LEDA* database

presented in our Fig. 4; for NGC 7606, NGC 7537, and NGC 7721, the V profiles are shown in Fig. 4, but due to poor seeing conditions ($\simeq 3.5''$), they are unreliable for $r \lesssim 5''$.

4. Global results and discussion

4.1. *Presentation of the results*

Greyscale images and isophotes of the galaxies are presented in K' and, when available, in B, J, and H, in Fig. 4 (Table 5 in Appendix B gives the lowest-level isophote for each object). Profiles are given for surface brightness (in one or more passbands: B, R, I, J, H, and/or K'), colors (when available), ellipticity, and position angle; profiles are also given for isophotal-shape coefficient e_4 (when it was possible to calculate its value at more than a couple of arcsec), and, for the four galaxies with JHK' observations, e_6 (*ibid*).

Table 2a collects the luminosity profiles (for convenience, we have added to our NIR data the B, R, and/or I data), the ellipticities and orientations; Table 2b lists the

Table 3. Results of the photometric analysis

#	object		PA	ϵ	J_T	H_T	K_T	$D_{25}(B)$	$D_{20}(J)$	$D_{19}(H)$	$D_{19}(K)$	$D_{20}(K)$
(1)	(2)	(3)	(4)	(5)	(6)	(7)	(8)	(9)	(10)	(11)	(12)	(13)
1	E 320-26		162	0.63	9.78	9.02	8.71	153.2	97.2	87.4	100.0	....
2	E 380-06		71	0.55			7.74	213.7			127.6	....
3	E 267-37	N 4219	30	0.65	9.20	8.36	8.10	197.7	134.4	127.7	133.3	....
4	E 322-28		111	0.58			10.36	86.0			37.1	61.0
5	E 323-38		178	0.52			10.29	80.2			46.5	58.3
6		N 5119	22	0.69			9.82	....			58.6	69.2
7		N 5604	10	0.41			9.71	....			45.0	62.8
8		M -2-38-22	104	0.43			10.03	....			33.8	53.3
9		M -1-39-05	26	0.42			10.60	....			41.0	58.7
10		N 5937	25	0.61			9.12	....			58.8	73.8
11		N 6063	168	0.34			....	....			24.4	43.2
12	E 139-11		88	0.67			10.05	91.5			43.1	53.7
13	E 140-24	I 4717	93	0.75			9.42	102.9			72.8	86.7
14	E 184-17	I 4821	5	0.58			10.24	117.0			55.5	79.5
15	E 184-27	I 4826	41	0.34			10.86	78.3			27.2	40.6
16	E 184-67	N 6788	71	0.66	9.82	8.84	8.53	175.3	98.2	99.6	105.8	....
17	E 142-35	N 6810	174	0.73	8.98	8.15	7.81	193.6	130.6	123.8	125.0	....
18	E 073-22	I 4929	20	0.75			11.09	111.3			49.4	58.0
19	E 233-41	N 6870	87	0.54			10.19	151.9			46.1	72.4
20	E 399-25		167	0.41			....	97.0			30.0	47.4
21	E 287-13		61	0.61			9.28	229.0			93.4	123.9
22	E 107-36	N 7083	16	0.45			8.23	224.4			90.9	130.8
23	E 466-38	N 7172	104	0.35			8.27	....			91.7	116.7
24		N 7328	88	0.65			9.50	....			60.4	93.5
25	E 290-29	I 5267	139	0.25			7.81	347.7			94.1	....
26	E 406-34	I 5271	139	0.62			8.22	162.6			113.9	142.3
27		N 7537	78	0.72			10.00	....			47.7	74.8
28		N 7541	98	0.73			8.44	198.3			131.7	....
29		N 7606	149	0.56			8.01	....			135.2	188.0
30	E 605-07	I 5321	50	0.40			11.35	76.3			16.3	35.6
31		N 7721	16	0.64			8.89	....			100.6	151.1

Columns:
(1)-(3): galaxy identification
(4) PA: position angle of outer isophotes (at $\mu_{K'} = 19.5$), in degrees, North through East
(5) ϵ: outer ellipticity (at $\mu_{K'} = 19.5$)
(6)-(8) J_T, H_T, K_T: total magnitudes in the J, H, and K (from K' data) bands
(9) $D_{25}(B)$: major axis in arcsec at $\mu_B = 25$, recomputed on ESO-LV images with a corrected sky brightness, when relevant
(10)-(13) $D_{20}(J)$, $D_{19}(H)$, $D_{19}(K)$, $D_{20}(K)$: major axis in arcsec at $\mu_J = 20$, $\mu_H = 19$, $\mu_K = 19$, and $\mu_K = 20$ (from K' data)

e_4 through e_8 coefficients. These two Tables are proposed in electronic form only.

Table 3 collects total magnitudes, parameters of outer isophotes, and isophotal radii. Also listed, for 20 objects, is the B-band D_{25} diameter from the ESO-LV images, recalibrated as explained in Sect. 3.

Tables 1, 2a, b and 3 are available from the CDS, Strasbourg, via anonymous ftp to 130.79.128.5.

4.2. *Surface photometry compared to other authors*

1. Brightness accuracy: from the catalog of Gezari et al. (1993), we collected the K-band aperture-photometry data available in the recent literature for six galaxies belonging to our sample (an additional object, NGC 7172, was eliminated due to obvious inconsistencies between the data from different sources and even within a single source). We performed simulated aperture photometry on our images, and Table 4 presents the results compared to previously published data, converted to K'. We found a mean difference of 0.038 ± 0.073, a reasonable agreement. For NGC 6810, we found an excellent agreement with the H and K (corrected to K') measurements of Griersmith et al. (1982: hereafter GHJ82), but we noticed a systematic discrepancy of 0.12 mag in J between their values and

ours. We also compared our profiles, for three galaxies

Table 4. Comparison with published aperture photometry

object	A	K'	Ref	$K'_{\rm mes}$	residual
(1)	(2)	(3)	(4)	(5)	(6)
IC 5267	21.8	9.16	GHJ82	9.03	−0.13
IC 5267	33.0	8.78	GHJ82	8.71	−0.06
IC 5267	56.0	8.38	GHJ82	8.33	−0.05
IC 5271	18.1	10.14	GHJ82	9.96	−0.18
IC 5271	30.1	9.48	GHJ82	9.35	−0.13
NGC 6810	12.0	9.18	GHJ82	9.18	0.00
NGC 6810	18.1	8.76	GHJ82	8.76	0.00
NGC 6810	30.1	8.36	GHJ82	8.38	0.02
NGC 7537	44.5	10.43	BRS84	10.35	−0.08
NGC 7541	44.5	9.26	BRS84	9.24	−0.02
NGC 7541	54.7	9.05	BRS84	9.07	0.02
NGC 7721	7.2	12.06	DEV89	12.15	0.09
NGC 7721	9.3	11.76	DEV89	11.78	0.02

Columns:
(1) galaxy identification
(2) A: aperture diameter (in arcsec)
(3) K': magnitude within A
(4) Ref: reference for Col. (3); BRS84: Bothun et al. (1984); DEV89: Devereux (1989); GHJ82: Griersmith et al. (1982)
(5) $K'_{\rm mes}$: our measured value for simulated aperture photometry within A
(6) residual: $K'_{\rm mes} - K'$

in common (NGC 7537, NGC 7541, and NGC 7606), with those of Terndrup et al. (1994), who also used ellipse fitting to the isophotes. We applied a suggested correction of 0.65 mag to their data (Terndrup, private communication), and another K-to-K' correction of 0.05 mag; we found a good agreement (Fig. 2), except for the innermost regions where resolution effects may be present, and for the intermediate region of NGC 7541 (between $\simeq 20''$ and $\simeq 30''$ from the center). Globally, if a systematic offset exists, it does not exceed 0.1 mag.

2. Determination of the major-axis position angle: we compared our measured values with those listed in the *LEDA* database, and we found for four objects (NGC 5604, NGC 5937, NGC 7721, and MCG -1-39-05), a significant discrepancy with the cited source (Corwin, to be published), in the sense that $\rm PA_{ours} + PA_{LEDA} \simeq 180°$. With these exceptions, the rms difference in the PA values is $\simeq 5°$ (we note that this figure includes the effect due to the difference in morphology between the NIR and visible domains).

4.3. *Morphology*

With $M_B \lesssim -19$, our galaxies are intrinsically bright; the sample is limited but, not surprisingly, the global characteristics statistically confirm what has recently been published on the NIR morphology (see, e.g., Block & Wainscoat 1991; Rix & Rieke 1993; Block et al. 1994; de Jong 1995; Rauscher 1995). Our main comments are the following:

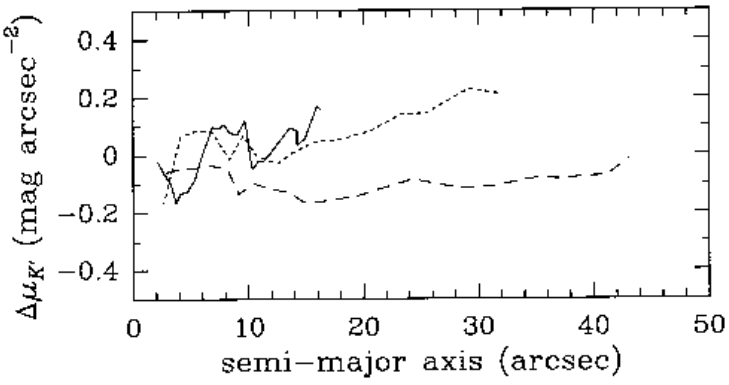

Fig. 2. Comparison of our K' photometric profiles with those of Terndrup et al. (1994), for the three galaxies in common. The magnitude difference $\Delta\mu_{K'} = \mu_{\rm (ours)} - \mu_{\rm (theirs)}$ is plotted as a function of the semi-major axis of the isophotes. *Solid line*: NGC 7537; *Dotted line*: NGC 7541; *Dashed line*: NGC 7606. Data at less than $2''$ from the center are not shown

- we found a conspicuous bar in three objects so far classified unbarred (ESO 323-38, MCG 1-39-05 and MCG 2-38-22), and there are five suspected other cases (IC 4821, IC 5271, NGC 5119, NGC 5604 and NGC 6063); the bars are much more frequent than can be estimated in the visible. But we also noted one opposite case (NGC 7541), where the barred structure seen in the visible is only an artifact of the obscuring pattern.
- three galaxies exhibit a central bright, flattened feature exactly aligned along the major axis, which is likely to be disky (ESO 320-26, NGC 6810, and NGC 7172); two other cases are more ambiguous (ESO 380-06 and NGC 7083). it is not clear whether this is only the inward prolongation of the main disk (made visible by the low extinction) or an independent inner structure. This question demands a thorough photometric analysis which is beyond the scope of the present paper; for one object, ESO 320-26, Héraudeau et al. (1995b: hereafter HSM95b) present evidence for an independent structure.
- the spiral pattern, sometimes blurred on images in the visible bands, is more contrasted, and its general aspect fits into the framework defined by Block et al. (1994). A few galaxies, however, exhibit particularly thin arms, which may deserve a closer attention (NGC 4219, NGC 7083, NGC 7541, NGC 7606, and MCG 2-38-22).
- photometric profiles often show the distinctive characteristic known as "Type II" (Freeman 1970): this is the case for at least 11 out of the 31 galaxies in our sample. It is sometimes more pronounced in the visible

than in the NIR (effect of the young population?), but it is sometimes the opposite (effect of dust?).

4.4. *Color-color diagrams*

For the four objects observed in three passbands, the angular resolution was sufficient to allow an examination of the color maps, and we wanted to use the color-color diagrams to get an insight on the obscuration by dust. We calculated the mean $(J-H)_0$ and $(H-K')_0$ indices integrated within ellipses fitted to the isophotes; the subscript 0 indicates values corrected for Galactic extinction (Rieke & Lebofsky 1985, and references therein), and redshift (K-correction: Longmore & Sharples 1982). The parameters of the ellipses were the same for the three colors; they were determined on the K'-band images, beginning at a semi-major axis of $2''$, with a step of $2''$. Our results are displayed in Fig. 3a.

We presented in Fig. 3b, for comparison, the diagrams corresponding to:

- aperture-photometry of elliptical galaxies from the compilation of de Vaucouleurs & Longo (1988); this represents 258 measurements at different apertures on 96 objects (the following three references gather $\simeq 70\%$ of these data: Aaronson 1977; GHJ82; Glass 1984). The same corrections as above were applied, together with a K-to-K' correction.
- aperture-photometry of spirals from the same compilation, selected for being non-AGN objects according to Véron-Cetty & Véron (1993): 435 measurements on 191 objects. A well-known characteristic, already noted by, e.g., GHJ82, Glass (1984), and Carico et al. (1984), is clearly present: the clustering of most of the data in a region of the graph close to that occupied by the elliptical galaxies; we may be able to add a point: that the mean shift from the elliptical to spiral barycenters corresponds to $A_V \lesssim 1$. Besides the accumulation of data in this region, the spirals also show a tail extending to the redder end of the diagram, and which corresponds to the inner regions of $\simeq 20\%$ of the galaxies (GHJ82; Glass 1984). Many galaxies of the *IRAS* minisurvey (Soifer et al. 1984; Rowan-Robinson et al. 1984) populate this tail (Carico et al. 1986; Moorwood et al. 1986, 1987); Seyfert galaxies occupy the lower envelope of the tail (GHJ82, and references therein; Kotilainen et al. 1992).

Compared to the data of Fig. 3b, our results for the four galaxies lead to the following comments:

- The global extent of the color-color loci, although not contained in the mean ellipse, is nevertheless close to it, and within a region populated by many other spirals. The four galaxies do not belong to the sample of the minisurvey, but they have $L_{\rm FIR}/L_B$ ratios within its range (although close to the lower limit), and they lie within the characteristic tail. NGC 4219, which is ranked second in $L_{\rm FIR}/L_B$ ratio, reaches the redder color indices, along both axes. NGC 6810, with the highest ratio, is found in the literature with either Seyfert-2 or starburst-nucleus classifications, and is well within the region of the diagram occupied by such objects.
- We may note (naively), that various physical processes and population effects are available for explaining the observed tracks in the color-color diagrams; there has been some evidence, however, that for normal and "nearly-normal" spirals, the JHK diagrams can, at least crudely, be interpreted in terms of reddening due

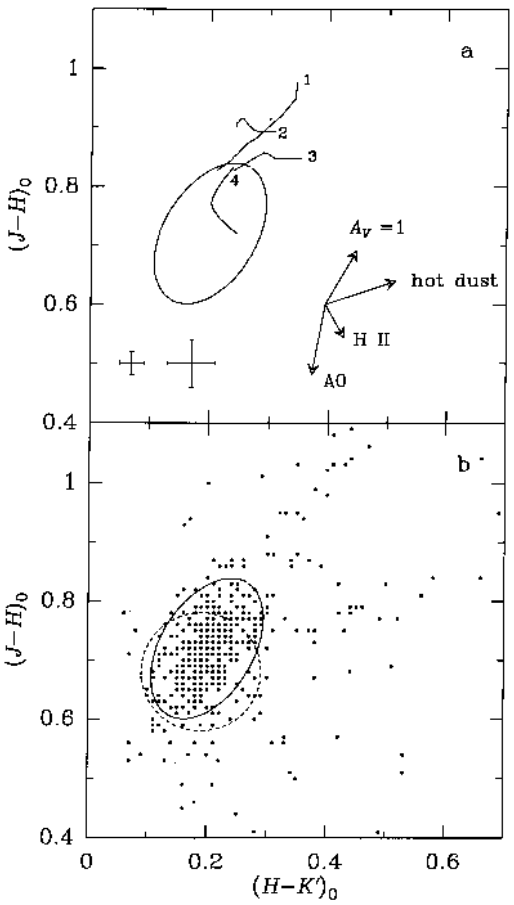

Fig. 3. Color-color diagrams. The indices are corrected for Galactic extinction and redshift. **a)** data for our four galaxies; *solid curves*: loci of color indices integrated within isophotes, the numbers are close to the innermost points and identify the objects (1, NGC 4219; 2, NGC 6788; 3, NGC 6810; 4, ESO 320-G 026); *error bars*: mean uncertainty on indices, at $20''$ and $40''$ from the center; *arrows*: effects of Galactic-law extinction, and 10% of flux from: hot (1000 K) dust, thermal bremsstrahlung (H II), and A0 stars (10 000 K blackbody); *ellipse*: mean area of non-AGN spirals. **b)** data from the literature; *points*: aperture photometry for non-AGN spirals from de Vaucouleurs & Longo (1988); *solid ellipse*: mean area; *dashed circle*: mean area corresponding to elliptical galaxies

to dust (GHJ82; Moorwood et al. 1986, 1987). Then, for at least three of our galaxies, the global extinction in the inner region can be estimated to roughly $A_V \lesssim 1$ or 2 mags.
- A more detailed analysis of the absorption patterns (dust lanes and patches), e.g. by using local color-color diagrams and a wider range of passbands, is beyond the scope of this work, and will be presented later (HSM95b).

4.5. *Discussion*

We have presented NIR surface photometry for a sample of 31 spiral galaxies, and comparison with (a few) other sources does not show significant systematic errors. Tables containing K'-band profiles (plus J and H for four selected objects), isophote parameters, B and R profiles (some of them corrected) from ESO-LV, and I profiles (mostly from Mathewson et al. 1992) are available in electronic form.

Morphological analysis confirms several global trends revealed by recent studies, concerning the aspect of the spiral pattern and the bar phenomenon. A brief look at color indices in the central region of the four objects with large angular dimension suggests extinction effects at a level not unexpected; these regions turned out to be rich in features like dust lanes, dust patches, crescent-shaped structures.

Our data are aimed at preparing the following applications:

1. The surface brightness will be analyzed in term of stellar components. Following Simien & Héraudeau (1994) and Héraudeau & Simien (1995: hereafter HS95), a decomposition into bulge, axisymmetric disk and spiral-arm contributions will be performed (Héraudeau et al. 1995a); the hypothesis that the "Freeman type II" profiles are associated to the spiral pattern (HS95; de Jong 1995) will be tested. And the inner bright disks, as observed in several members of our sample, will deserve particular attention. Our results will be compared to recent other works, e.g., Peletier et al. (1994), and de Jong (1995) for face-on galaxies.
2. The mass models resulting from the photometric decomposition will be used to generate rotation curves to be compared to Hα and H I measurements (Héraudeau et al. 1995a). Taking advantage of a) the better mass dependence of the NIR surface brightness in the central and intermediate regions (Rix & Rieke 1993), and, b) the farther-reaching B, R, or I data in the outer regions, should allow a fair estimate of the "visible" mass; constraints on the amount of dark matter will then result.
3. Multi-band data, from B to K', will be used to investigate extinction effects in more detail, and central features will be studied individually (HSM95b).

Acknowledgements. We thank R.F. Peletier and E.A. Valentijn for their valuable advice on infrared techniques prior to our observing run. We are indebted to R.F. Peletier who, as the referee, made numerous comments that helped to improve the manuscript. We are also pleased to thank D. Mathewson and V. Ford for providing us with their data in digital form, the ESO-ST/ECF Archive Service for extracting images from the ESO-LV database, and Ph. Prugniel and E. Pécontal for helpful discussions. This research was sponsored in part by a grant (to G.A.M.) from the GdR Cosmologie (CNRS). The *LEDA* extragalactic database is operated by G. Paturel and the Lyon and Meudon Observatories.

Appendix A.

Comments on individual objects:

1. **ESO 320-26**: pointed innermost isophotes ($e_4 \simeq 0.04$), providing evidence for a bright central disk; this inner structure appears too bright to be the inward prolongation of the main disk (HSM95b). Boxy bulge structure? "Type II" photometric profile.
2. **ESO 380-06**: boxy bulge. Possible inner disk.
3. **ESO 267-37 / NGC 4219**: outer warp visible on the B image; two-armed inner spiral pattern, with emergence of arms at $\simeq 4''$ from the nucleus. Thin main spiral arms. Evidence for a compact bulge surrounded by a crescent-shaped structure of diameter $\simeq 7''$ parallel to the major axis. "Type II" profile.
4. **ESO 322-28**: many foreground stars superposed. Bright, compact bulge. "Type II" profile in B and R, not in K'.
5. **ESO 323-38**: its structure appears rather patchy for a K'-band image. Evidence of a bar of diameter $\simeq 4''$ aligned with outer disk. "Type II" profile.
6. **NGC 5119**: spiral arms almost parallel to the major axis. Possibly barred. May have been classified too late at T=5. "Type II" profile.
7. **NGC 5604**: may be slightly barred, although classified SAa. And a later type may be more appropriate. "Type II" profile.
8. **MCG 2-38-22**: thin bar, with thin arms starting from its extremities and winding for almost 180°. Very compact bulge.
9. **MCG 1-39-05**: thin, elongated bar.
10. **NGC 5937**: although a short $m = 2$ pattern dominates the spiral structure, a third arm is clearly apparent; overall patchy aspect, unusually similar to a visible-band image.
11. **NGC 6063**: poor S/N ratio, but a "grand-design" spiral pattern is detectable. Compact bulge. Possible inner bar.
12. **ESO 139-11**: observed during critical weather conditions, and a cloud is visible on the frame, although not on the object itself. Compact bulge. Too small for detailed morphological analysis. "Type II" profile.
13. **ESO 140-24 / IC 4717**: the PSF turned out to be asymmetric. Highly inclined. Suspected ringed

structure (barely visible) or, conversely, spiral pattern mimicking a ring. "Type II" profile.

14. **ESO 184-17 / IC 4821**: many superposed stars. The elongated central condensation has not exactly the same orientation as the major axis, and may be a bar; this is not visible on the B and R images.
15. **ESO 184-27 / IC 4826**: only the central region is available on our K' image. No apparent structure.
16. **ESO 184-67 / NGC 6788**: emergence of embryonic spiral arms at $r \simeq 5$ ″; inside, the bulge position angle is very close to that of the outer disk, suggesting an oblate geometry. No evident continuity of the spiral arms.
17. **ESO 142-35 / NGC 6810**: highly inclined. In B, large-scale dust lane parallel to the major axis, and overall patchy appearance. In the NIR, complex central structure, with i) pointed innermost isophotes, giving evidence for a bright disk here, ii) a crescent-like bright feature at $\simeq 5''$ on the far side (barely visible in B), which turned up to be the unobscured half of the innermost bulge region (HSM95b), iii) the emergence of two spiral arms, and iv) a large bulge, whose outer regions distort the outermost disk isophotes (this far-reaching bulge is markedly different from the one visible in B on the ESO-LV image; see, e.g., Simien et al. 1993).
18. **ESO 073-22 / IC 4929**: imperfect flatfielding. Highly inclined object, strongly asymmetric along the major axis, a characteristic also conspicuous on the ESO-LV images. Very dusty in B and R; in K', two symmetric inner arms are clearly visible. "Type II" profile.
19. **ESO 233-41 / NGC 6870**: amorphous disk structure. The bright, compact inner bulge is significantly dimmed on the B image.
20. **ESO 399-25**: imperfect flatfielding; nevertheless, the profile seems reliable down to $\mu_{K'} \simeq 19.5$. No apparent structure.
21. **ESO 287-13**: observed with imperfect focusing. Shows marginal evidence of incipient spiral structure starting at $r \simeq 5''$. Indication of "type II" profile.
22. **ESO 107-36 / NGC 7083**: thin spiral structure; on our image, it is difficult to make a choice between the following two interpretations: either a two-armed structure winding for more than 180°, or a shorter two-armed structure branching into a four-armed one at $\simeq 10''$ from the center. Bright, compact bulge; slightly pointed innermost isophotes ($e_4 \simeq 0.03$), providing marginal evidence for a bright central disk.
23. **ESO 466-38 / NGC 7172**: nearly edge-on galaxy, with a strong absorbing lane in B parallel to the major axis (extinction $\Delta\mu_B \simeq 2$). In K', the lane is barely visible; bright central disk (inner isophotes with $e_4 \simeq 0.07$).
24. **NGC 7328**: asymmetric arms; faint bulge.
25. **ESO 290-29 / IC 5267**: dusty, low-contrast spiral pattern in B, invisible in K' (more akin an elliptical in this band).
26. **ESO 406-34 / IC 5271**: featureless in B. In K', at $r \simeq 7''$, marginal evidence for either the emergence of spiral arms or the presence of a bar. The disk is not very smooth. Photometric profile down to $\mu_{K'} = 22$. "Type II" profile.
27. **NGC 7537**: diffuse; very faint bulge (classified too late?).
28. **NGC 7541**: nearly edge-on, with a strong absorbing lane in B. Classified SB, but we see no evidence for a bar. Strong asymmetry along the two semi-major axes; thin asymmetric arms; compact bulge. "Type II" profile?
29. **NGC 7606**: multiple, tightly-wound thin spiral arms. Small bulge for a type T=3. "Type II" profile.
30. **ESO 605-07 / IC 5321**: the innermost profile only could be accurately measured (out to $r \simeq 15''$).
31. **NGC 7721**: asymmetric arms. Highly flattened bulge, or bar oriented along the major axis? "Type II" profile.

Appendix B.

Table 5 presents the brightness of the faintest isophotes displayed in the images of Fig. 4, in mag arcsec^{-2}.

References

Aaronson M., 1977, PhD Thesis, Harvard University

Bersanelli M., Bouchet P., Falomo R., 1991, A&A 252, 854

Block D.L., Bertin G., Stockton A., et al., 1994, A&A 288, 365

Block D.L., Wainscoat R.J., 1991, Nat 353, 48

Bothun G.D., Romanishin W., Strom S.E., Strom K.M., 1984, AJ 89, 1300

Carico D.P., Soifer B.T., Beichman C., et al., 1986, AJ 92, 1254

Carter B.S., 1993, in: Kilkenny, Lastivicia & Menzies (eds.), Precision Photometry, Proceedings of a Conference to honor A.J.W. Cousins, p. 100

de Jong R.S., 1995, PhD Thesis, University of Groningen

de Jong R.S., van der Kruit P.C., 1994, A&AS 106, 451

de Vaucouleurs A., Longo G., 1988, Catalogue of visual and infrared photometry of galaxies from 0.5 μm to 10 μm (1961-1985), The University of Texas Monographs in Astronomy, No. 5

Devereux N.A., 1989, ApJ 346, 126

Engels D., Sherwood W.A., Wamsteker W., Schultz G.V., 1981, A&AS 45, 5

Freeman K.C., 1970, ApJ 160, 811

Gezari D.Y., Schmitz M., Pitts P.S., Mead J.M., 1993, Catalog of infrared observations (third edition), NASA Ref. Publ. 1294

Glass I.S., 1984, MNRAS 211, 461

Griersmith D., Hyland A.R., Jones T.J., 1982, AJ 87, 1106 (GHJ82)

Héraudeau Ph., Simien F., 1995, Astro. Lett. Comm. 31, 219 (HS95)

Héraudeau Ph., Simien F., 1996, A&AS (in press) (HS96)

Table 5. Faintest-level isophotes in Fig. 4

#	object		B_f	J_f	H_f	K'_f
1	E 320-26		22.0	19.0	18.5	18.0
2	E 380-06		22.0			17.5
3	E 267-37	N 4219	23.0	19.5	18.5	18.0
4	E 322-28		22.5			18.5
5	E 323-38		23.0			18.5
6		N 5119				18.5
7		N 5604				18.5
8		M -2-38-22				18.5
9		M -1-39-05				18.0
10		N 5937				18.5
11		N 6063				19.0
12	E 139-11		22.5			18.5
13	E 140-24	I 4717	23.0			19.0
14	E 184-17	I 4821	22.0			18.5
15	E 184-27	I 4826	22.5			19.0
16	E 184-67	N 6788	22.5	19.5	18.5	18.5
17	E 142-35	N 6810	22.5	20.0	19.0	18.5
18	E 073-22	I 4929	22.0			19.0
19	E 233-41	N 6870	21.5			18.5
20	E 399-25		23.0			19.0
21	E 287-13		22.0			18.0
22	E 107-36	N 7083	21.5			18.0
23	E 466-38	N 7172	22.5			18.0
24		N 7328				18.0
25	E 290-29	I 5267	21.5			17.5
26	E 406-34	I 5271	22.0			18.0
27		N 7537				18.5
28		N 7541	22.0			18.0
29		N 7606				17.5
30	E 605-07	I 5321	22.0			18.5
31		N 7721				18.0

Héraudeau Ph., Simien F., Mamon G.A., 1995a, in: Rix H.-W. & Minniti D. (eds.) Spiral galaxies in the near infrared. ESO, Garching (in press)

Héraudeau Ph., Simien F., Mamon G.A., 1995b, in: Rix H.-W. & Minniti D. (eds.) Spiral galaxies in the near infrared. ESO, Garching (in press) (HSM95b)

Huizinga J.E., 1994, PhD Thesis, University of Groningen

Kotilainen J.K., Ward M.J., Boisson C., et al., 1992, MNRAS 256, 125

Kotilainen J.K., Prieto M.A., 1995, A&A 295, 646

Lauberts A., Valentijn E.A., 1989, The surface photometry catalogue of the ESO-Uppsala galaxies. ESO, Garching

Longmore A.J., Sharples R.M., 1982, MNRAS 201, 111

Longo G., de Vaucouleurs A., 1983, A general catalogue of photoelectric magnitudes and colors in the *U, B, V* system of 3578 galaxies brighter than the 16th *V* magnitude (1936-1982). The University of Texas Monographs in Astronomy, No. 3

Mathewson D.S., Ford V.L., Buchhorn M., 1992, ApJS 81, 413

McLeod K.K., Rieke G.H., 1995, ApJ (in press)

Michard R., Simien F., 1988, A&AS 74, 25

Moorwood A.F.M., Véron-Cetty M.-P., Véron P., Glass I.S., 1986, A&A 160, 39

Moorwood A.F.M., Véron-Cetty M.-P., Véron P., Glass I.S., 1987, A&A 184, 63

Moorwood A.F.M., Finger G., Biereichel P., et al., 1992, The Messenger 69, p. 61

Peletier R.F., Valentijn E.A., Moorwood A.F.M., Freudling W., 1994, A&AS 108, 621

Rauscher B.J., 1995, AJ 109, 1608

Rieke G.H., Lebofsky M.J., 1985, ApJ 288, 618

Rix H.-W., Rieke M., 1993, ApJ 418, 123

Rowan-Robinson M., et al., 1984, ApJ 278, L7

Simien F., Morénas V., Valentijn E.A., 1993, A&A 269, 111

Simien F., Héraudeau Ph., 1994, La Lettre de l'OHP 13, p. 1

Soifer B.T., et al., 1984, ApJ 278, L71

Tammann G.A., Sandage A., 1985, ApJ 294, 81

Terndrup D.M., Davies R.L., Frogel J.A., DePoy D.L., Wells L.A., 1994, ApJ 432, 518

Véron-Cetty M.P., Véron P., 1993, A catalogue of quasars and active nuclei (6th edition). ESO, Garching

Wainscoat R.J., Cowie L.L., 1992, AJ 103, 332

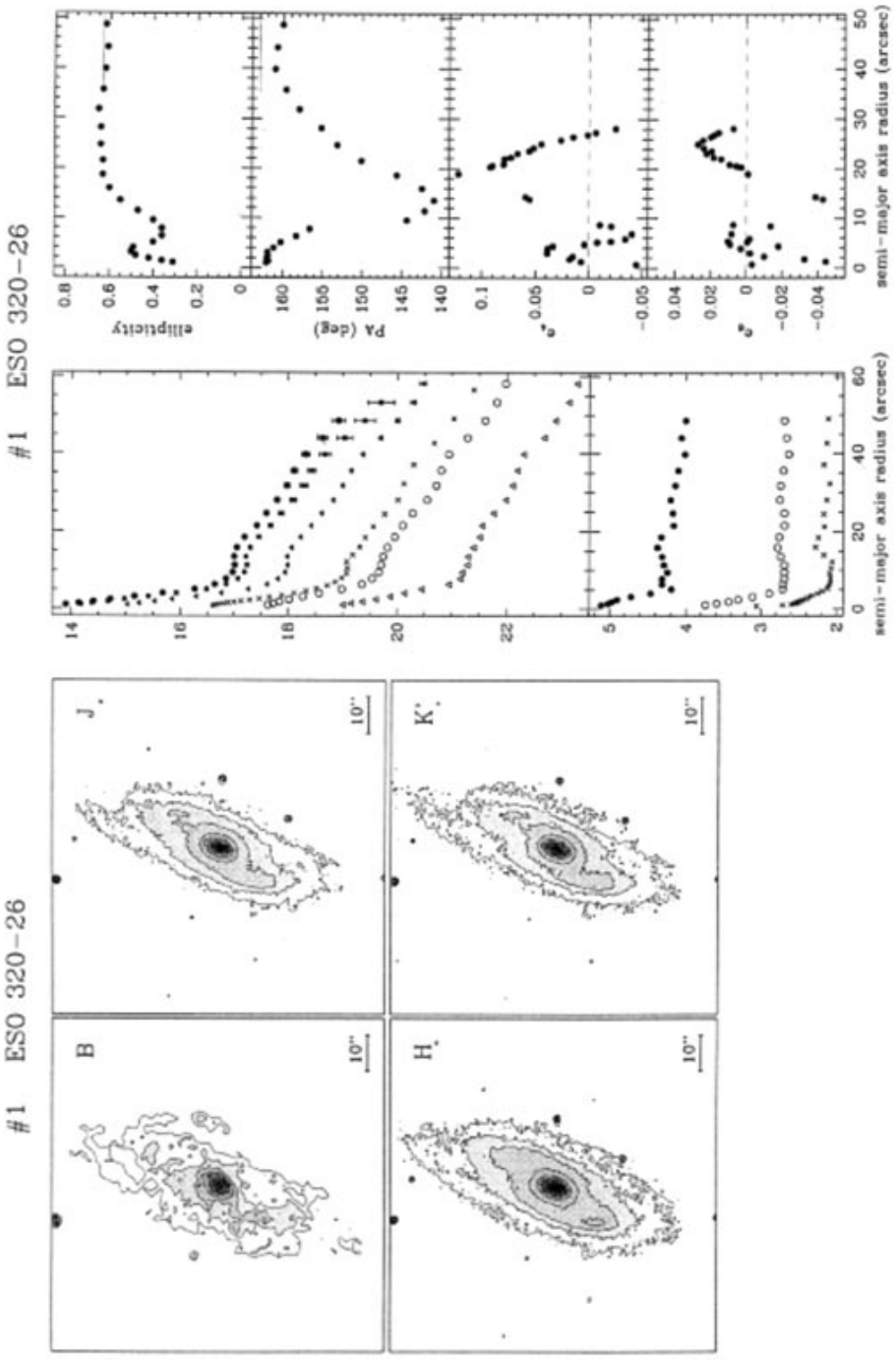

Fig. 4. Individual galaxies. **Greyscales**: B image (from ESO-LV, when available, with pixel size $1.35''$; from HS96 for galaxy #28, NGC 7541, with pixel size $0.78''$) and K' image; for four objects, J and H images are also given. North is on top and East is to the left. Contours and greylevels are spaced at integer and half-integer values of surface magnitude. Faintest isophotes are listed in Table 5 and chosen to produce high signal-to-noise contours in all bands and similar extension. **Surface brightness profiles**: $\mu_{K'}$ (*full circles*), and when available, μ_B (*open triangles*, from ESO-LV), μ_V (*open squares*, from HS96), μ_R (*open circles*, from ESO-LV), μ_I (*crosses*, from Mathewson et al. 1992, except for galaxy #28, which is from HS96), μ_J (*full squares*), μ_H (*full triangles*). Error bars are only given for the NIR profiles. **Color profiles**: when available, $B-K'$ (*full circles*), $V-K'$ (*open squares*), $R-K'$ (*open circles*), $I-K'$ (*crosses*). **Isophote-parameter profiles** (for K' isophotes): ellipticity ϵ, position angle PA, e_4 (when available), and also e_6 for the four large galaxies with JHK' data. Ellipticity and position angle from *LEDA* are shown as *thin horizontal lines* on right-hand side of plot. **(To be seen in landscape)**

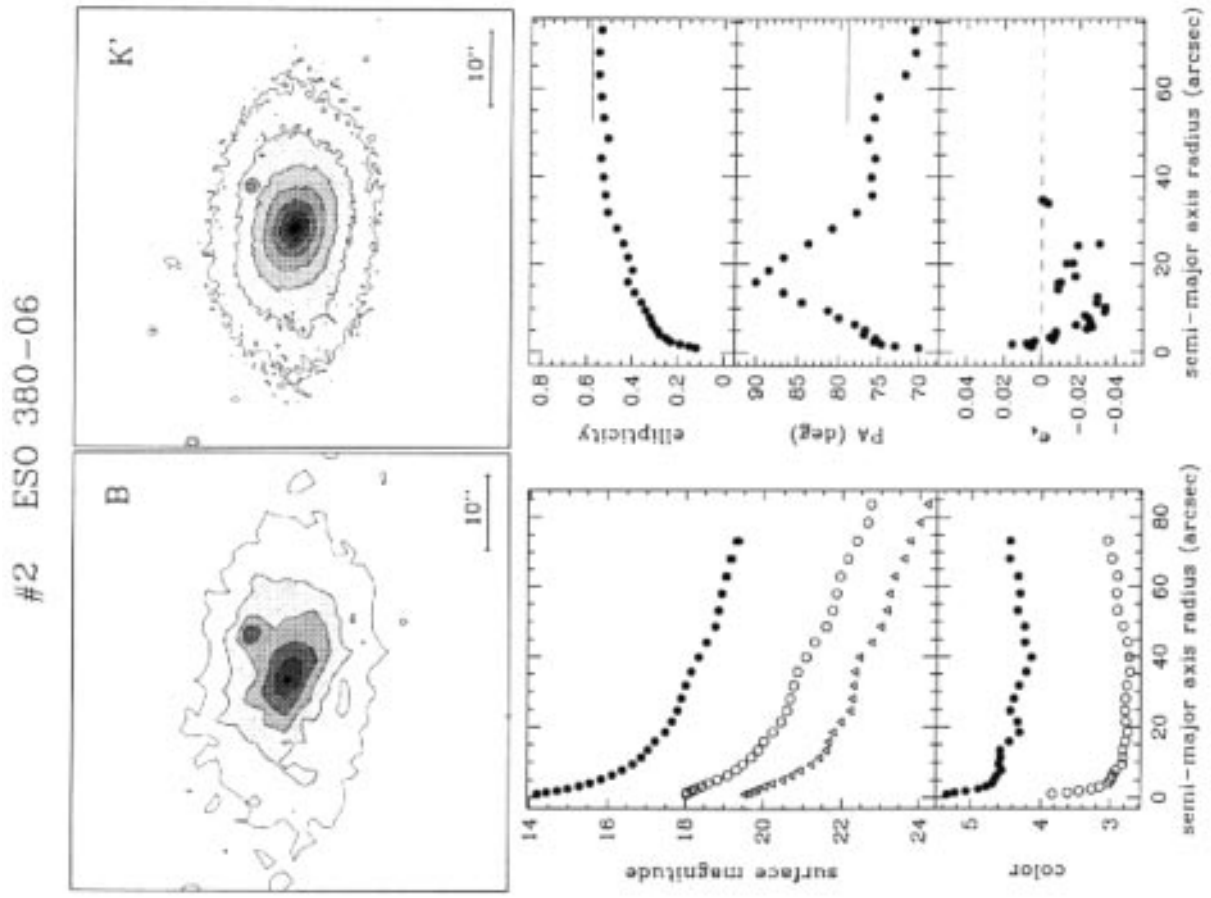

Fig. 4. continued. **(To be seen in landscape)**

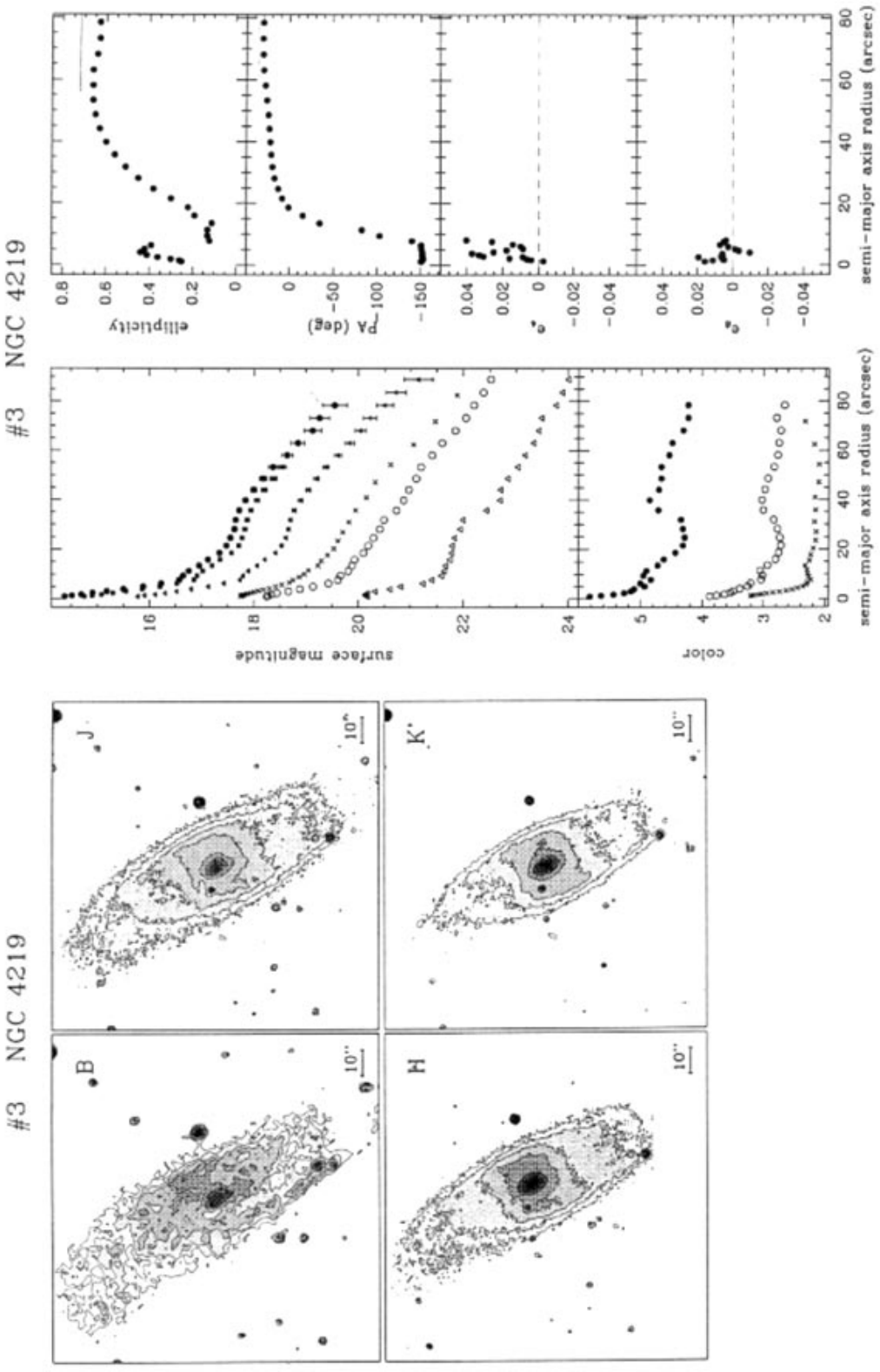

Fig. 4. continued. **(To be seen in landscape)**

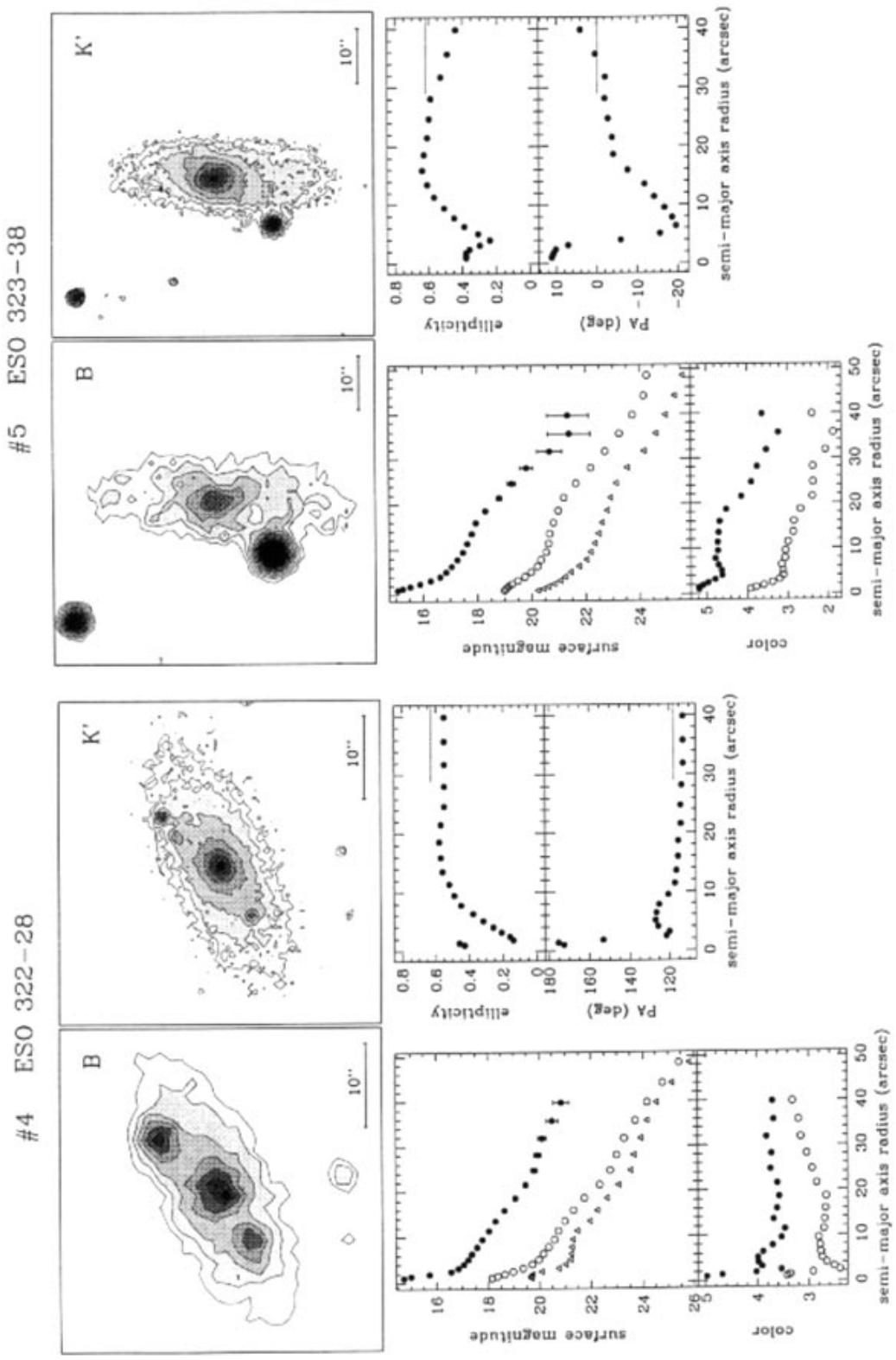

Fig. 4. continued. **(To be seen in landscape)**

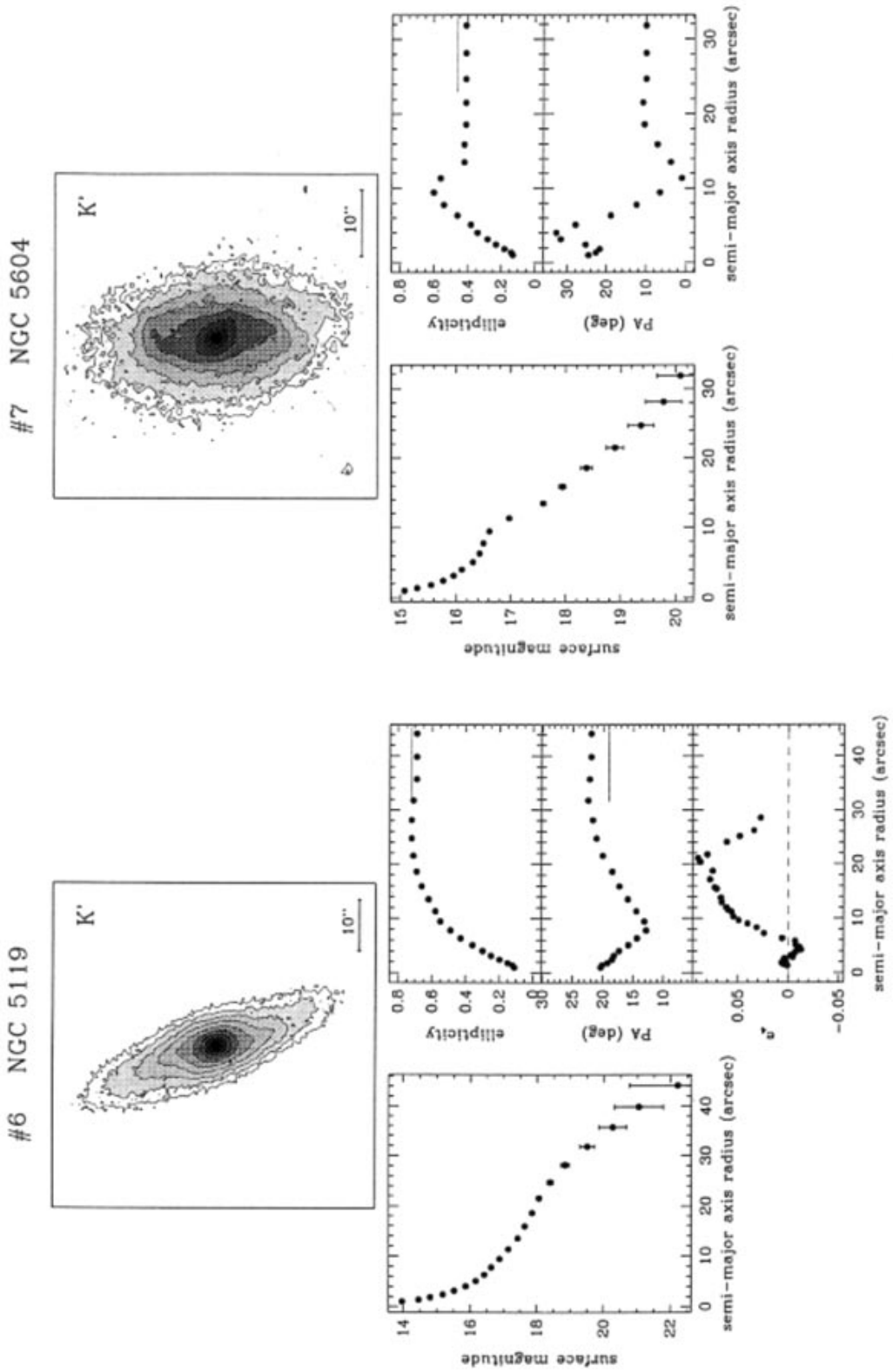

Fig. 4. continued. **(To be seen in landscape)**

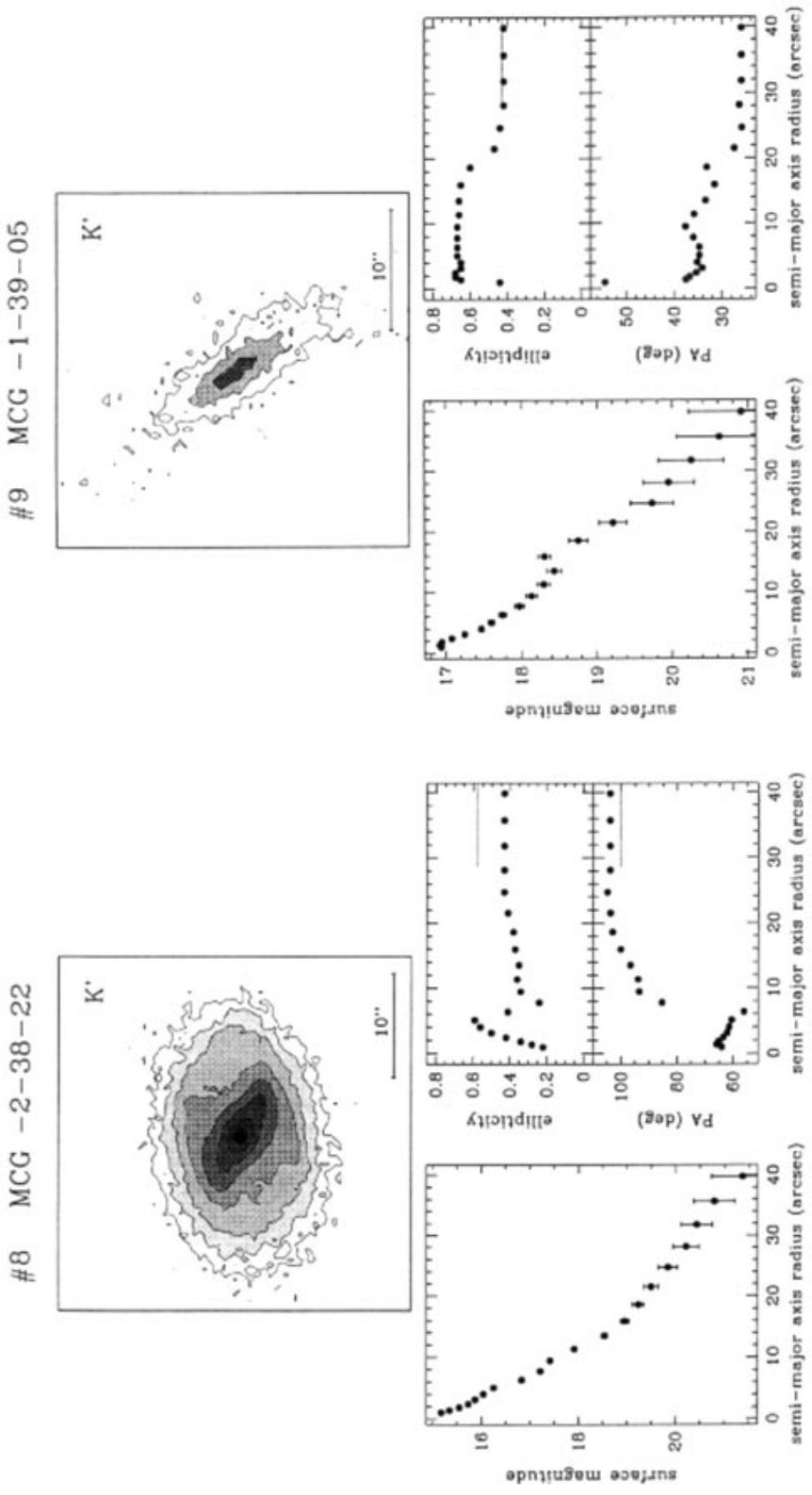

Fig. 4. continued. **(To be seen in landscape)**

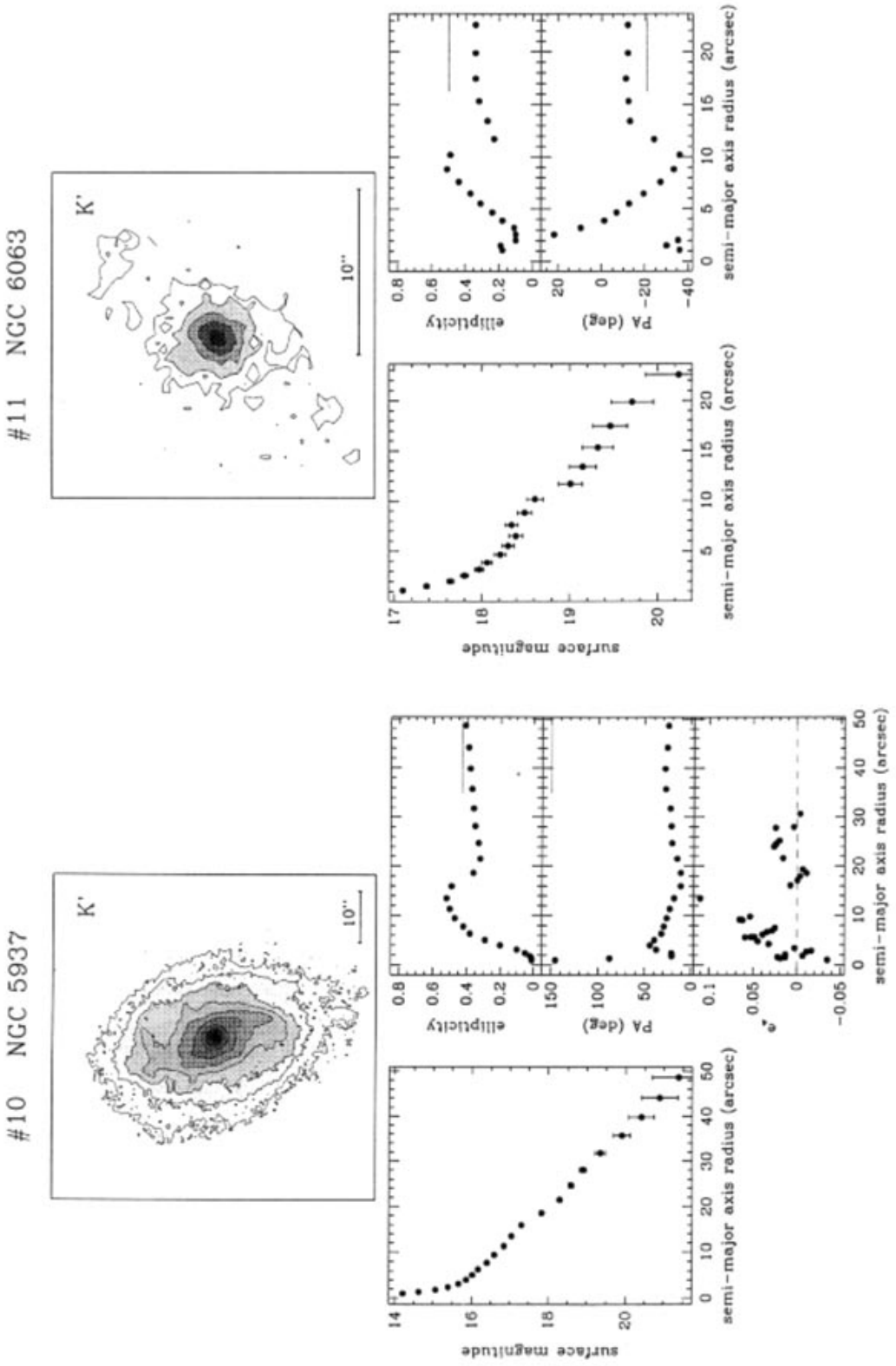

Fig. 4. continued. **(To be seen in landscape)**

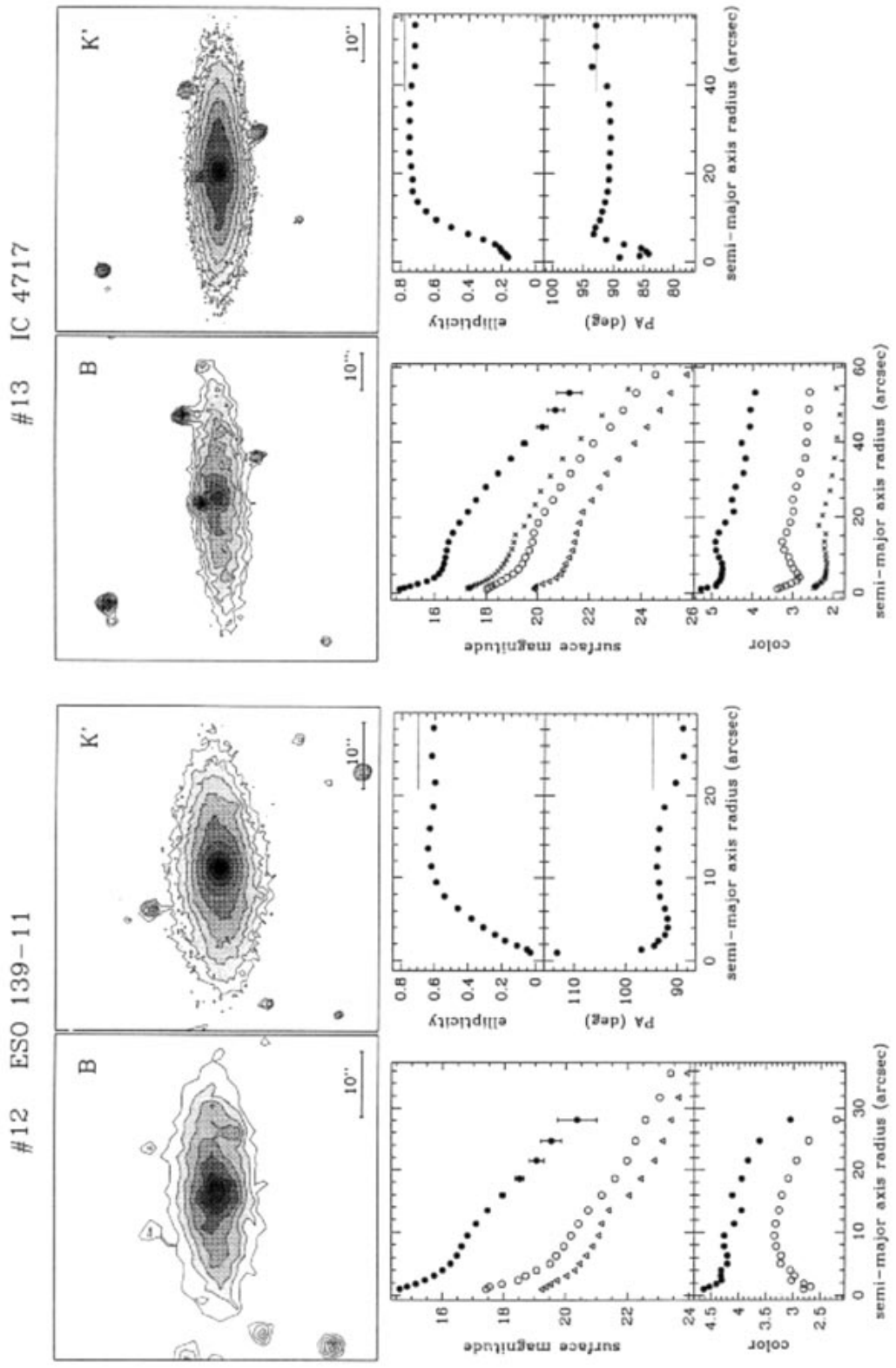

Fig. 4. continued. **(To be seen in landscape)**

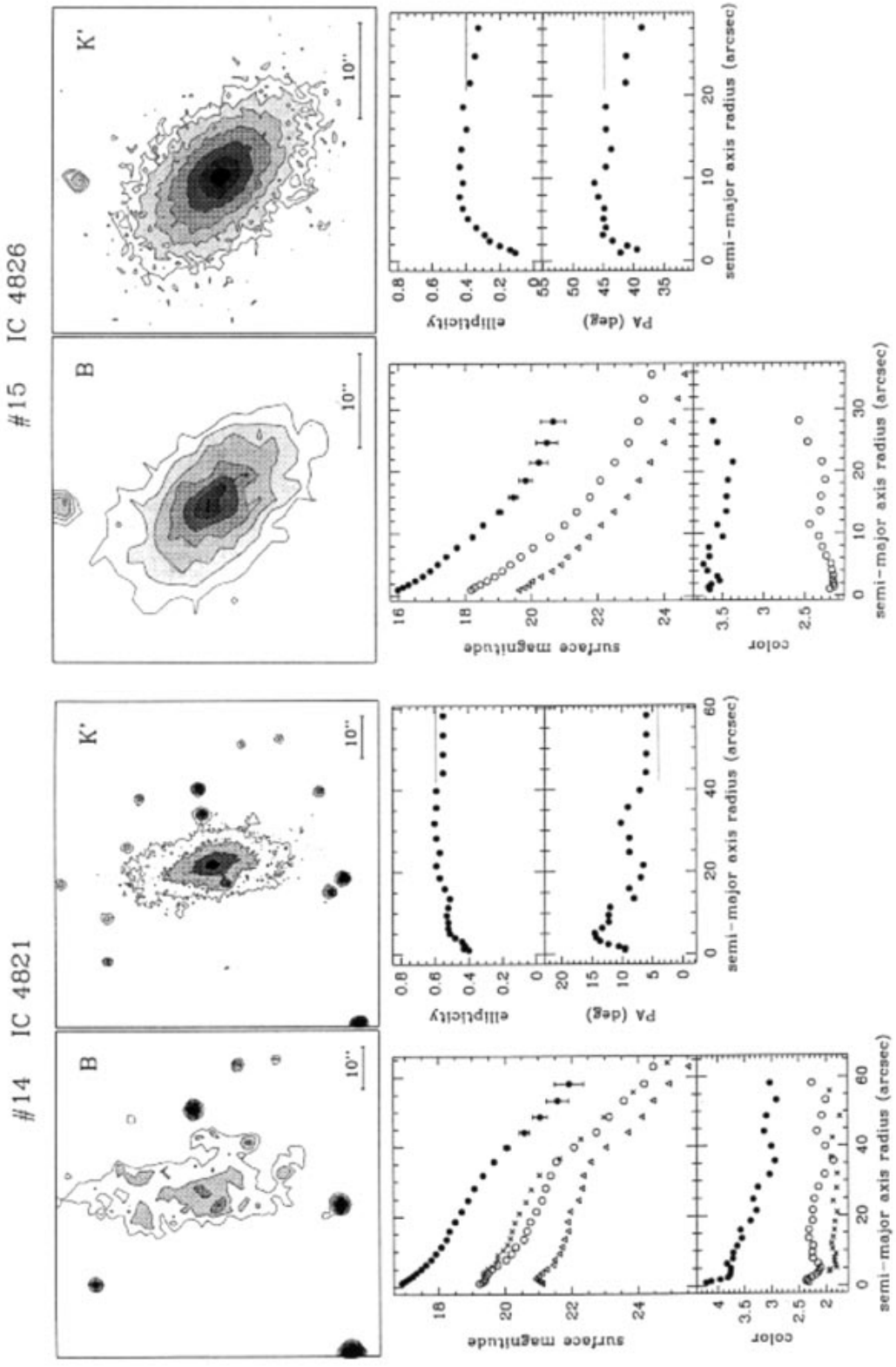

Fig. 4. continued. **(To be seen in landscape)**

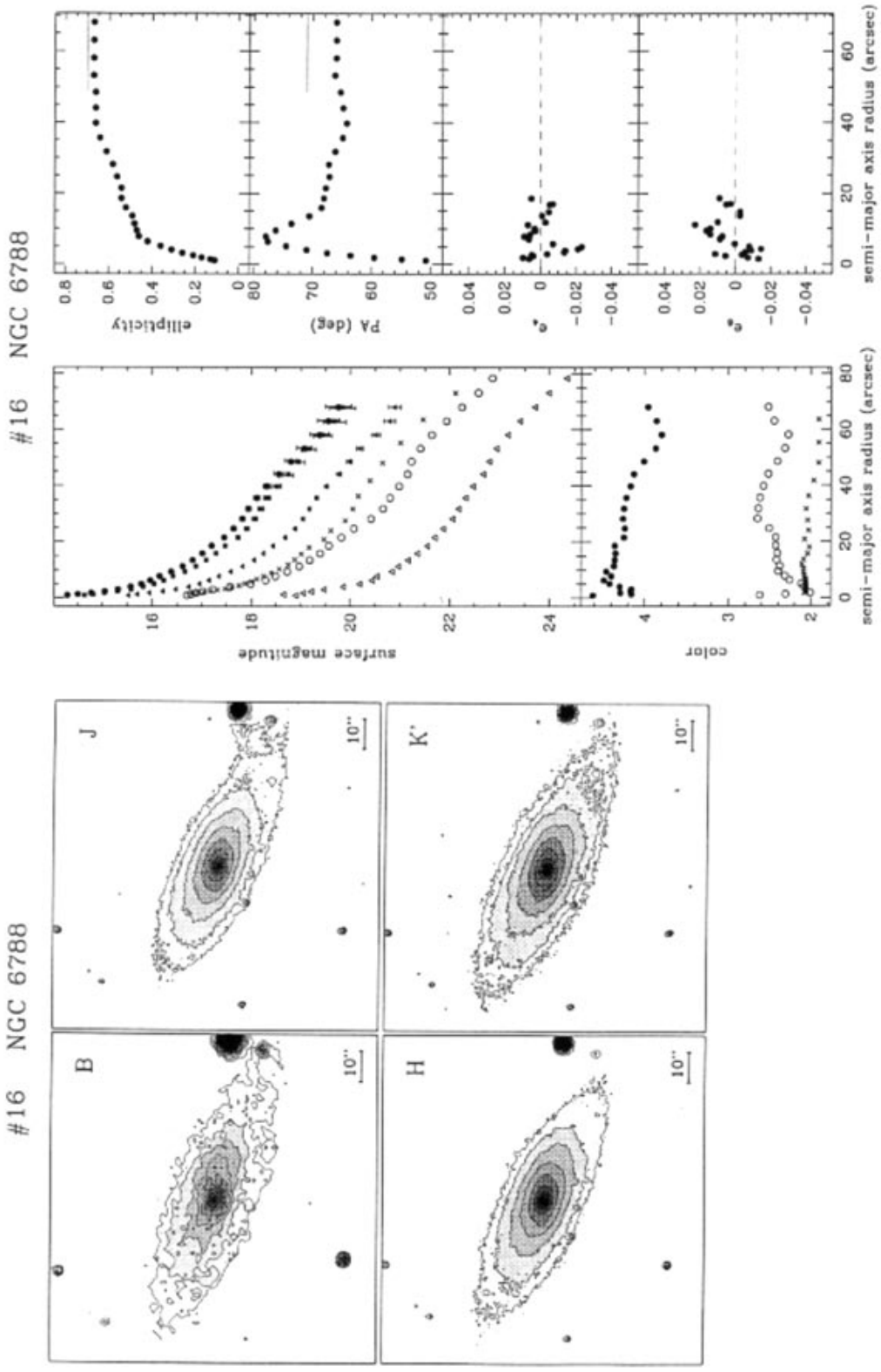

Fig. 4. continued. **(To be seen in landscape)**

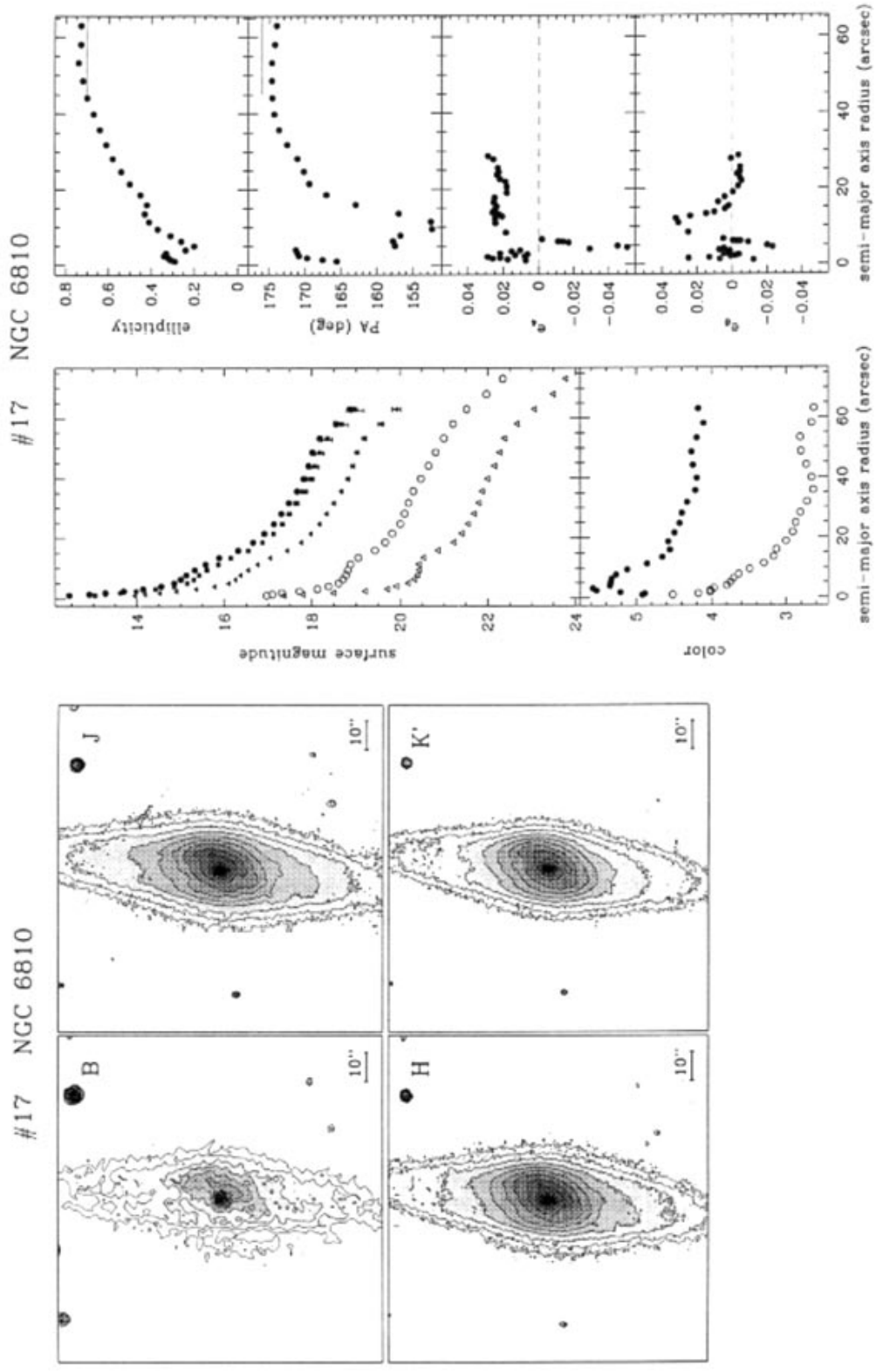

Fig. 4. continued. **(To be seen in landscape)**

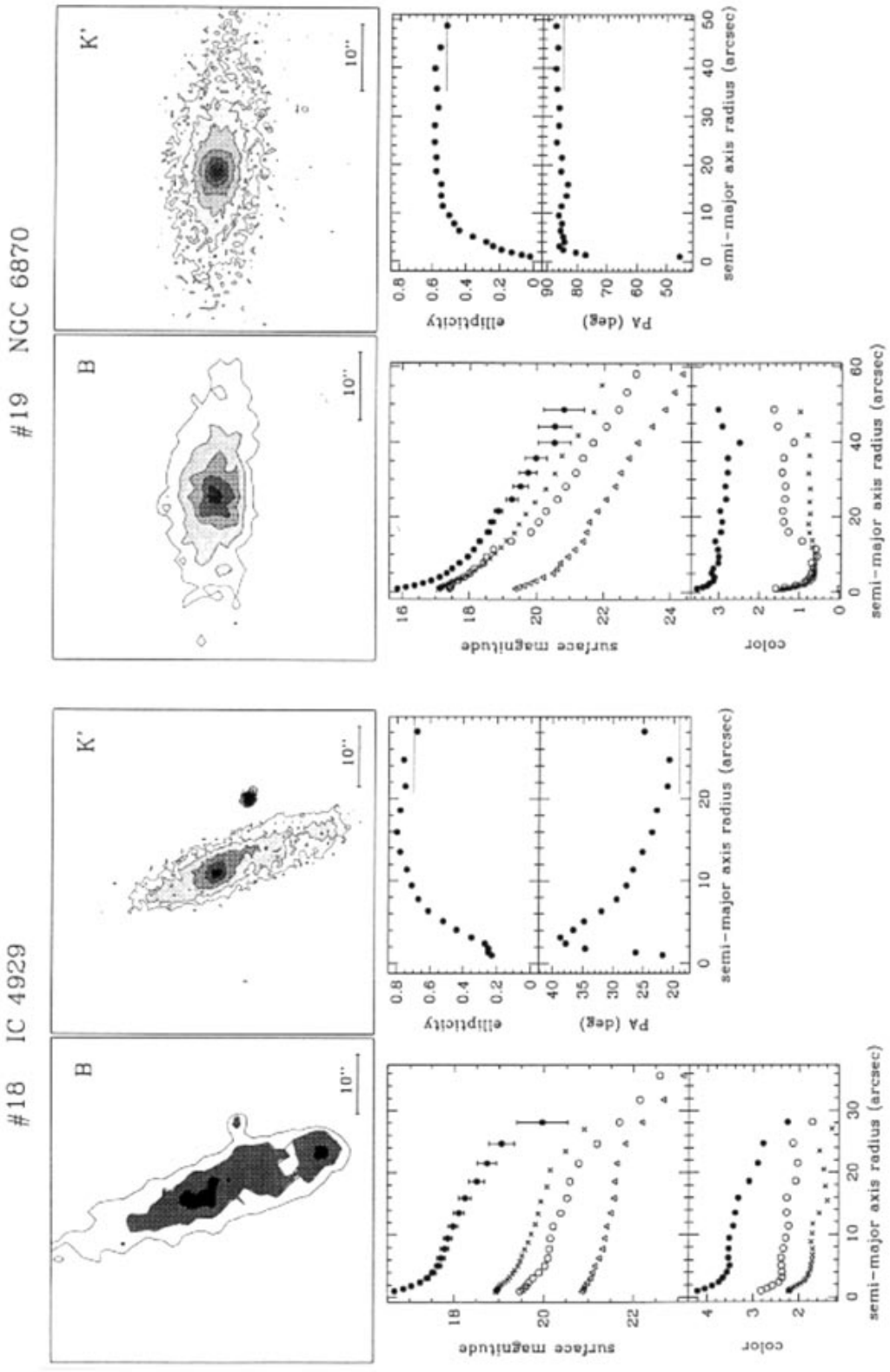

Fig. 4. continued. **(To be seen in landscape)**

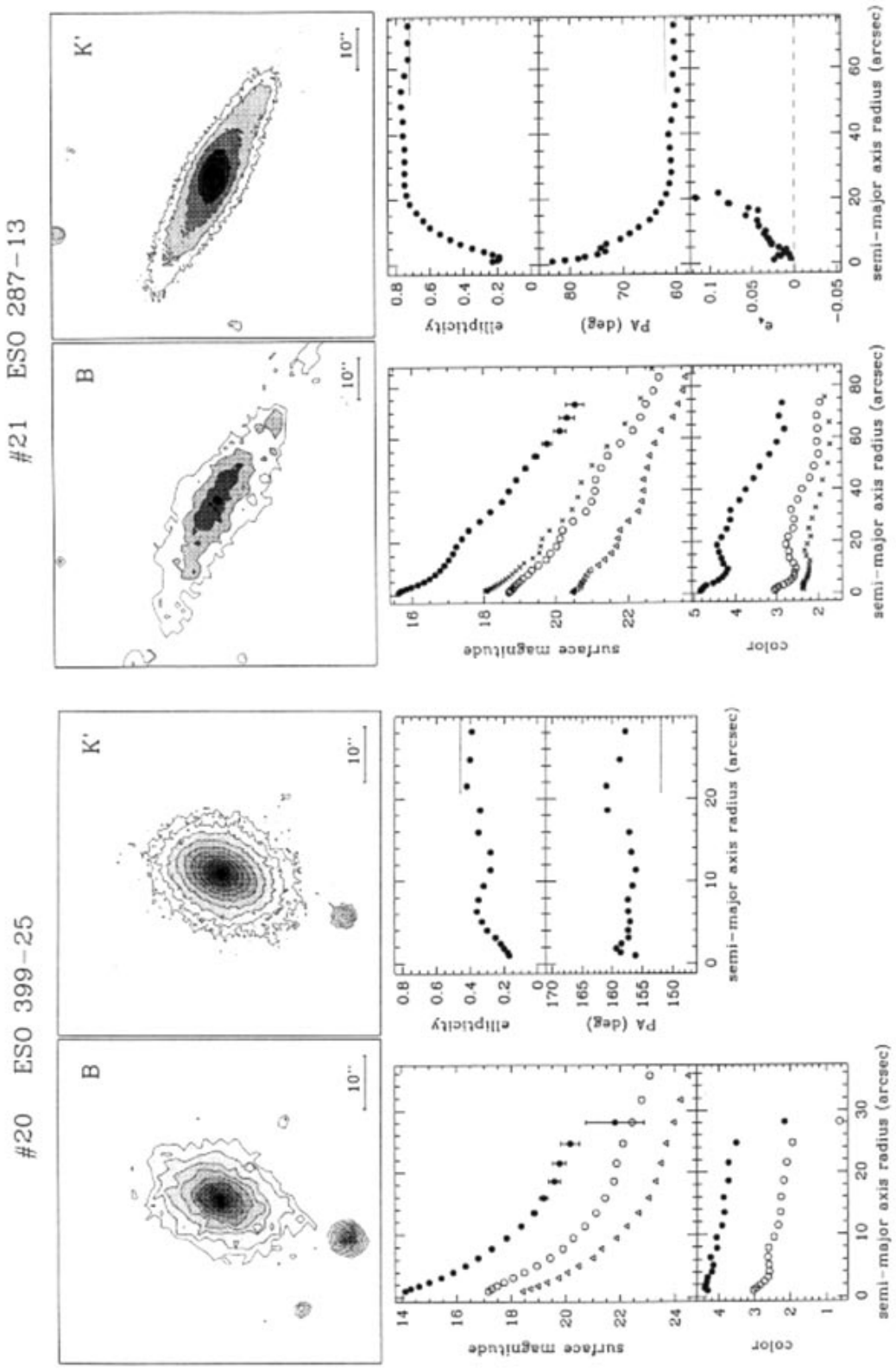

Fig. 4. continued. **(To be seen in landscape)**

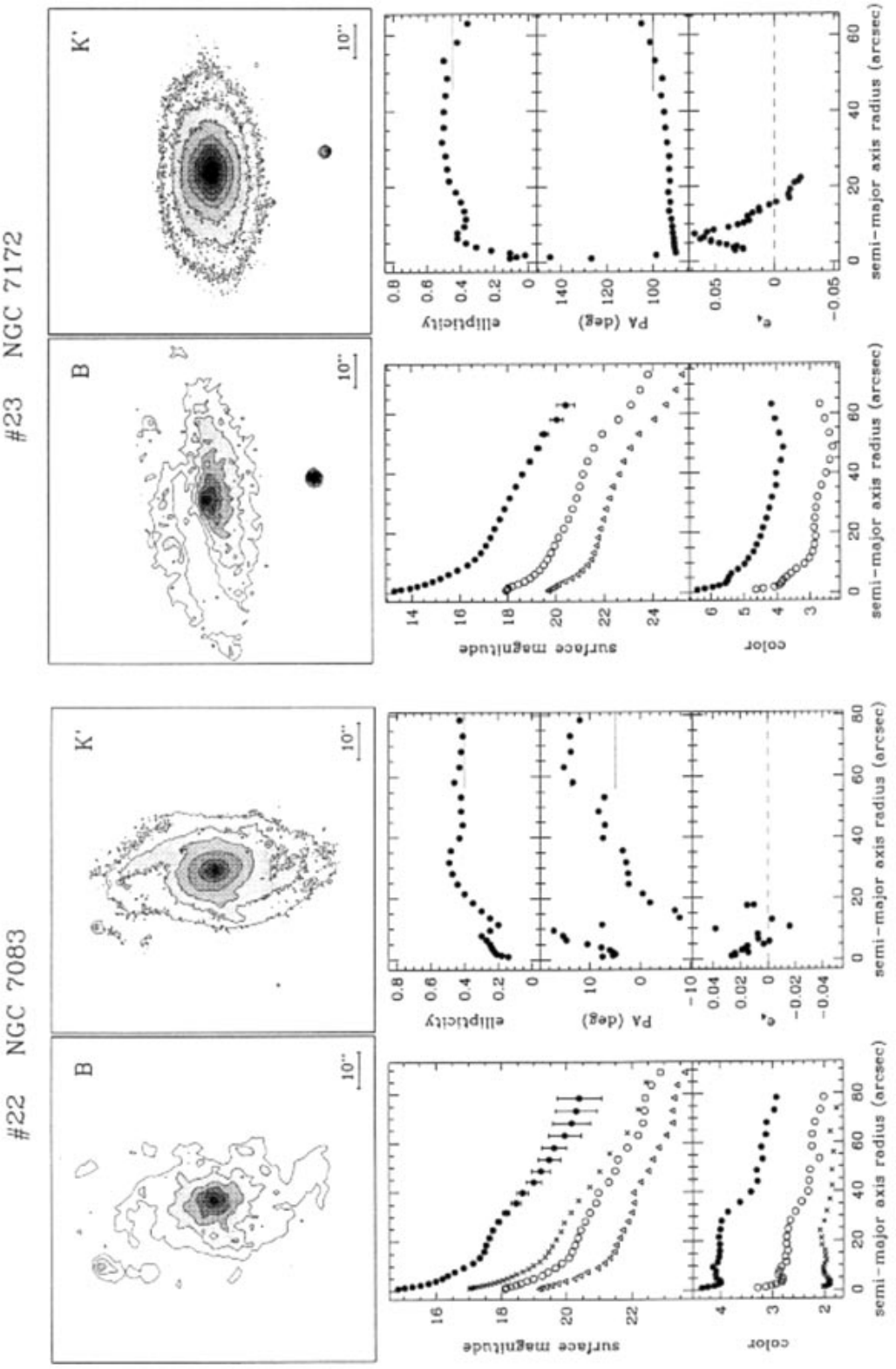

Fig. 4. continued. **(To be seen in landscape)**

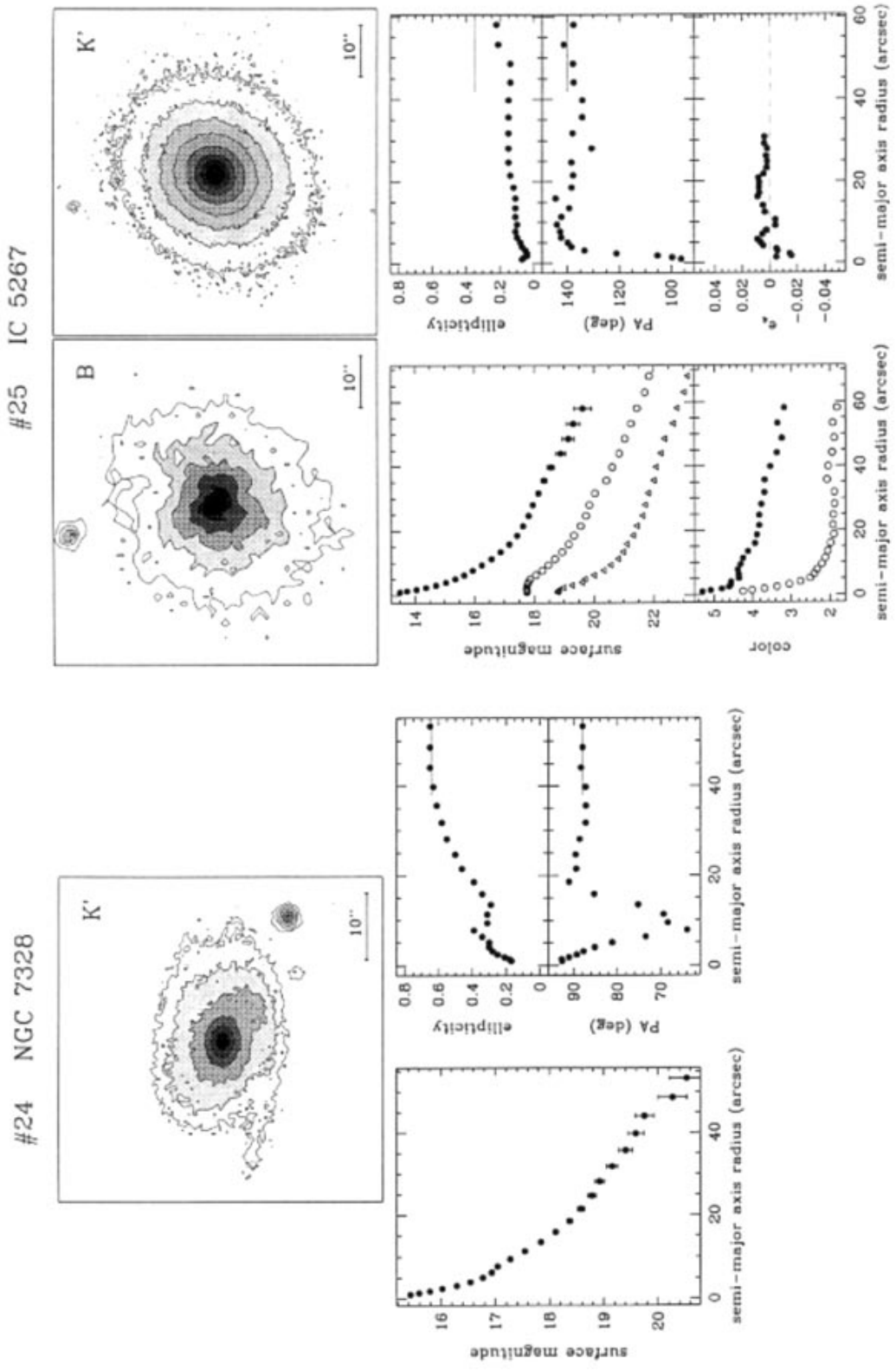

Fig. 4. continued. **(To be seen in landscape)**

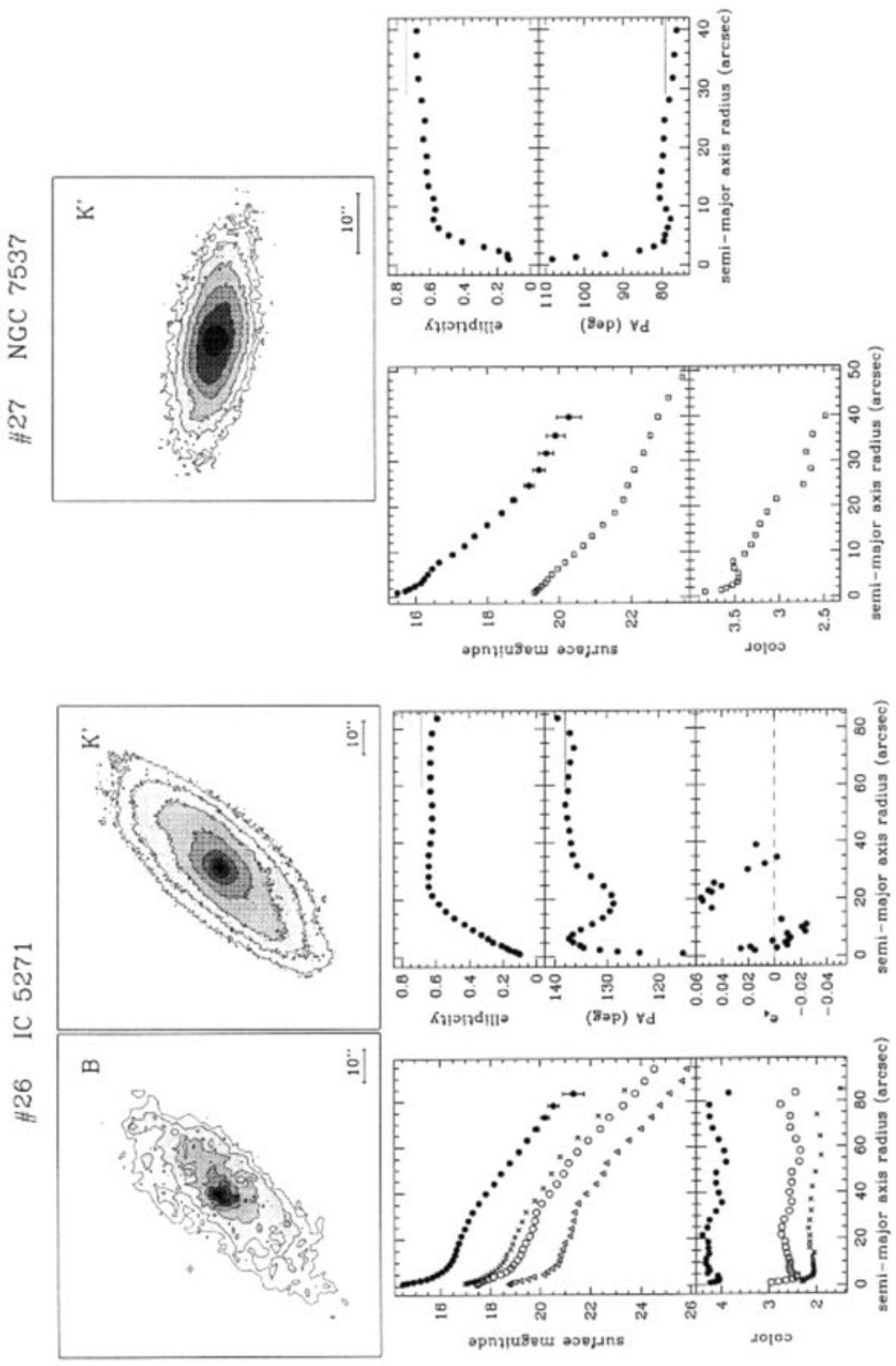

Fig. 4. continued. **(To be seen in landscape)**

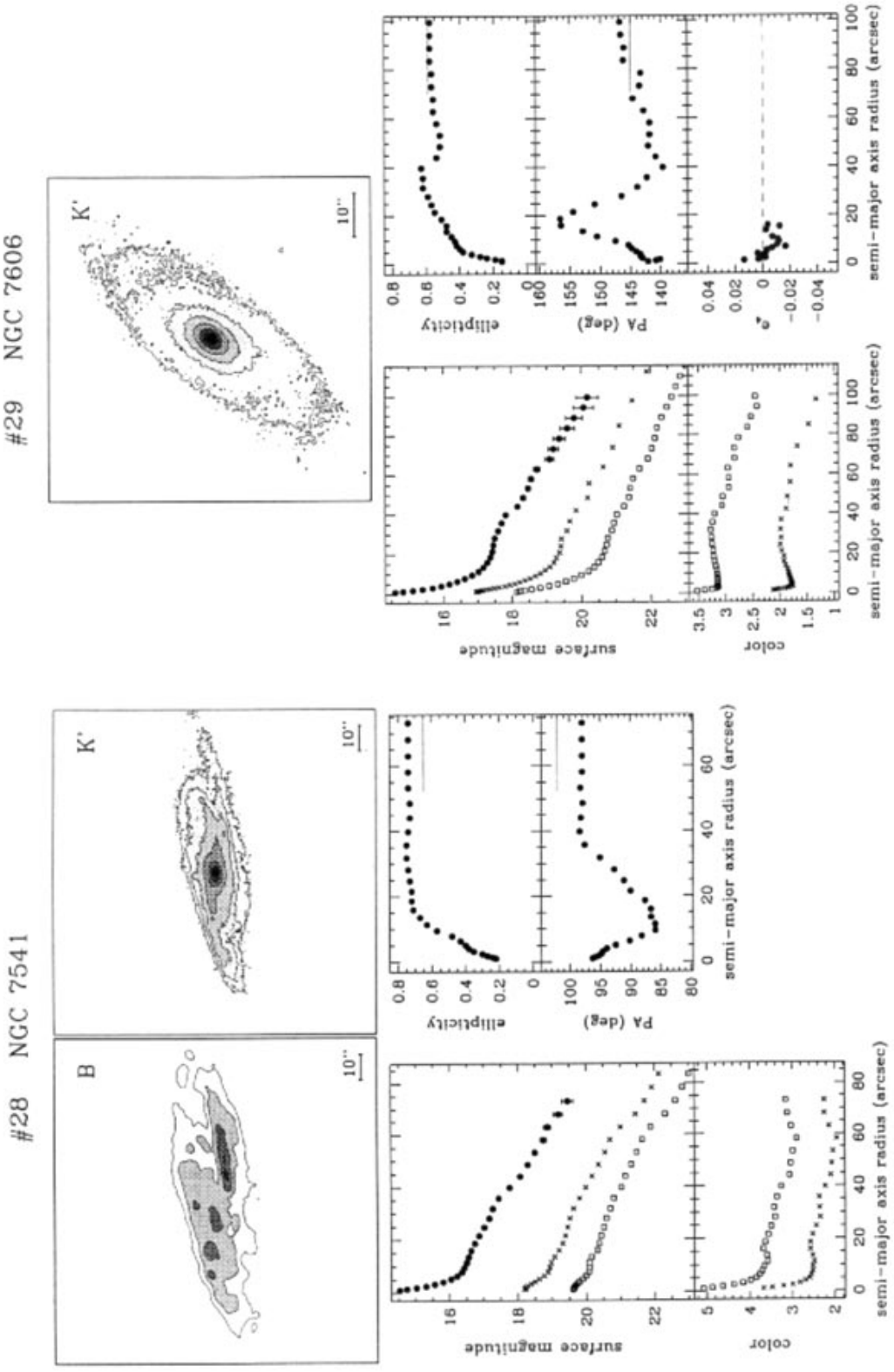

Fig. 4. continued. **(To be seen in landscape)**

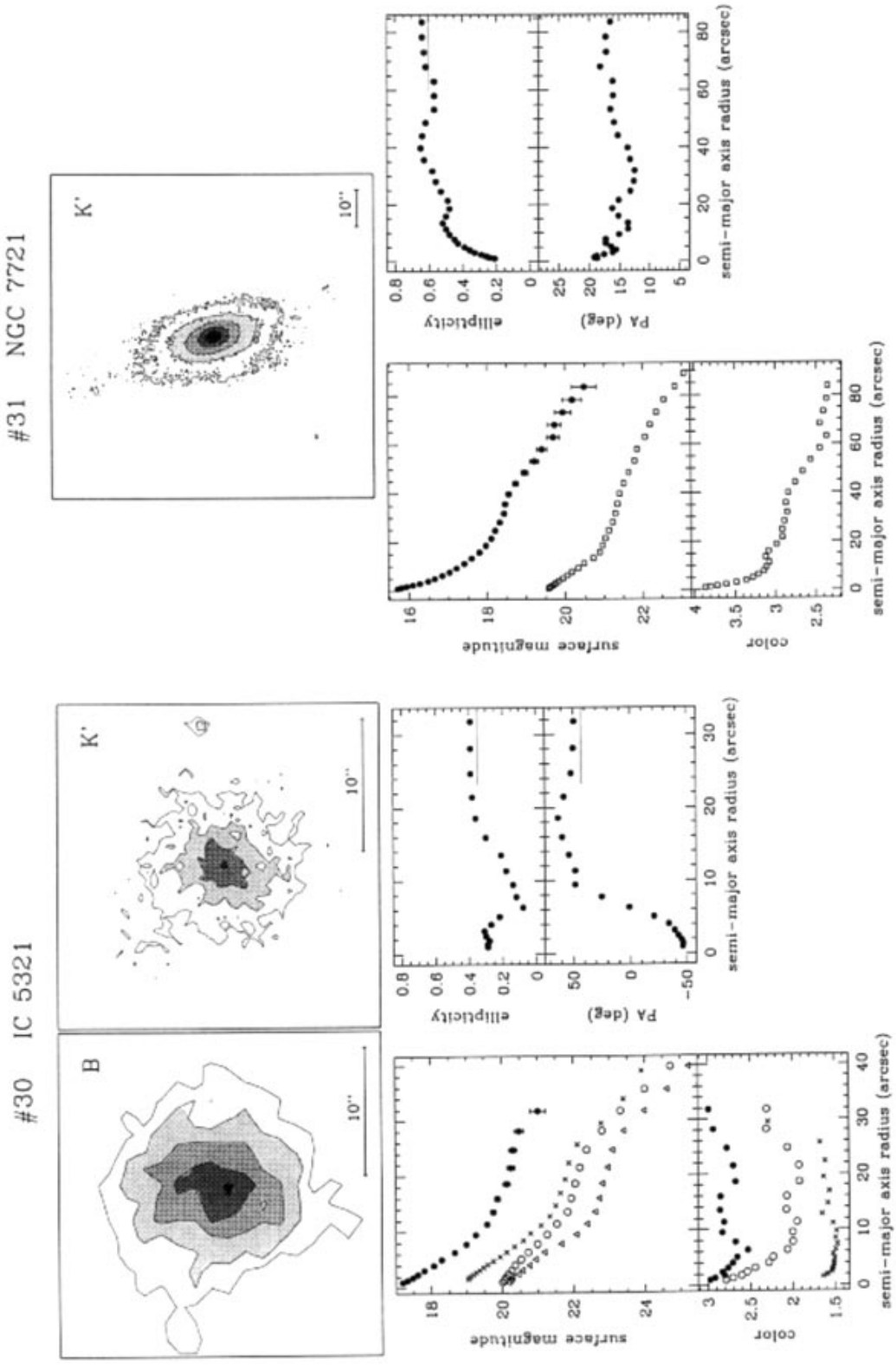

Fig. 4. continued. **(To be seen in landscape)**